Simultaneous observations of flux transfer events by THEMIS, Cluster, Double Star and SuperDARN: Acceleration of FTEs

R. C. Fear[1], S. E. Milan[1], A. N. Fazakerley[2], K.-H. Fornaçon[3], C. M. Carr[4] and I. Dandouras[5]

24th October 2009

An edited version of this paper was published by AGU.

Citation: Fear, R. C., S. E. Milan, A. N. Fazakerley, K.-H. Fornaçon, C. M. Carr and I. Dandouras (2009), Simultaneous observations of flux transfer events by THEMIS, Cluster, Double Star and SuperDARN: Acceleration of FTEs, *J. Geophys. Res.*, **114**, A10213, doi:10.1029/2009JA014310.

[1]Department of Physics & Astronomy, University of Leicester, Leicester, LE1 7RH, United Kingdom.
[2]MSSL, University College London, Holmbury St. Mary, Dorking, Surrey, RH5 6NT, United Kingdom.
[3]Institut für Geophysik und Extraterrestrische Physik, Technische Universität Braunschweig, Germany.
[4]Blackett Laboratory, Imperial College, Prince Consort Road, London, SW7 2BZ, United Kingdom.
[5]CESR/CNRS, 9 Avenue du Colonel Roche, B.P. 4346, 31028 Toulouse Cedex 4, France.

Correspondence to: r.fear@ion.le.ac.uk

Abstract

We present simultaneous observations of flux transfer events (FTEs) made by the THEMIS and Cluster spacecraft on 3 May 2007, along with supporting observations of fast flows in the dayside ionosphere observed by the SuperDARN radar network. The THEMIS spacecraft were in a string-of-pearls formation approximately 20,000 km long, and crossed the post-noon magnetopause at low latitudes between 12:00 UT (TH-C) and 14:30 UT (TH-E). The Cluster spacecraft were situated in the magnetosheath at high latitudes in the Southern Hemisphere, approaching the magnetopause which was crossed at about 16:00 UT. THEMIS observed 'standard' polarity FTE signatures between 11:00 and 15:00 UT, whilst Cluster observed 'reverse' polarity signatures at the same time. The two sets of signatures are consistent with being generated at the same small region of a subsolar reconnection line. Between 11:00 and 12:30 UT, the Double Star TC-1 satellite was near the magnetopause closer to local noon but still $\sim$7 R_E from the subsolar point. TC-1 only observed a single FTE, suggesting that the variability of the reconnection rate differed between these two locations on the X-line. Fast poleward ionospheric flows were observed in the noon- and prenoon sector, at similar magnetic local times to the footprints of both Cluster and THEMIS, after 12:00 UT. The long string formation of the THEMIS constellation allows the motion of the FTE structures to be tracked, and the acceleration is found to be small but consistent with a model prediction.

1 Introduction

Flux transfer events, or FTEs (*Russell and Elphic*, 1978, 1979), are bursts of magnetic reconnection (*Dungey*, 1961) at the Earth's magnetopause. The signature of an FTE observed by a spacecraft near the magnetopause consists of a bipolar variation in the component of the magnetic field normal to the magnetopause (B_N), and is often accompanied by an enhancement or a 'crater' in the magnetic field magnitude (*Paschmann et al.*, 1982). Such signatures may be caused either by the entry of a spacecraft onto the magnetic structure formed by reconnection, or simply by observing the draped field lines around the structure. If only the draping signature is observed, there is no change to the plasma parameters. If the spacecraft enters onto open magnetic field lines, then field-aligned plasma signatures characteristic of the opposite side of the magnetopause are also observed (*Daly et al.*, 1981, 1984): in a magnetospheric FTE, a cool, dense magnetosheath population will be observed moving along the magnetic field away from the magnetopause (this population may mirror at lower altitudes causing a bi-directional population to be observed); in a magnetosheath FTE, escaping hot, rare plasma is observed.

At the dayside magnetopause, FTE signatures are observed predominantly when the IMF has a southward component (*Rijnbeek et al.*, 1984; *Berchem and Russell*, 1984). When the IMF is northward, reconnection may occur at high latitudes (*Dungey*, 1963), and FTEs are then observed at the post-terminator magnetopause (*Kawano and Russell*, 1997a,b; *Fear et al.*, 2005). The ionospheric signatures of FTEs are observed at the footprints of newly opened field lines, and take the form of optical and radar auroral features and fast ionospheric flows, which are sometimes pulsed (*Sandholt et al.*, 1986, 1992; *Elphic et al.*, 1990; *Pinnock et al.*, 1993, 1995; *Moen et al.*, 1995; *Provan et al.*, 1998; *Milan et al.*, 1999a,b, 2000; *McWilliams et al.*, 2000, 2004; *Neudegg et al.*, 2001; *Wild et al.*, 2001, 2007; *Amm et al.*, 2005). Ionospheric observations can provide information about the global scale and rate of reconnection, whereas in situ satellite observations probe the small-scale structure. Observations of ultra violet and radar auroral features have shown that ionospheric reconnection signatures can extend over several hours of local time (*Milan et al.*, 2000). Magnetopause observations of FTE signatures by spacecraft at large separations have shown that FTEs occur both as large-scale features and smaller, more patchy events (*Fear et al.*, 2008, 2009).

If an FTE is observed by more than one spacecraft, then difference(s) in the time of observation of the magnetic field signatures and the known separation(s) of the spacecraft can be used to determine components of the FTE velocity. Several studies have applied such multi-spacecraft techniques (*Russell et al.*, 1983; *Harvey*, 1998) to FTEs observed by the four-spacecraft Cluster mission (*Escoubet et al.*, 2001) in order to study the motion of FTEs, and therefore the motion of open magnetic field lines at the magnetopause, in three dimensions (*Owen et al.*, 2001; *Wild et al.*, 2005; *Dunlop et al.*, 2005; *Fear et al.*, 2005). Some of the uncertainties in this method were examined by *Fear et al.* (2007), but one assumption that was not addressed was the assumption that the velocity of the FTE is constant as it crosses the spacecraft constellation. The recent launch of the THEMIS mission (*Angelopoulos*, 2008) has allowed observations of FTE structure at larger scales than those hitherto available with Cluster, although only in one dimension (*Sibeck et al.*, 2008; *Liu et al.*, 2008; *Lui et al.*, 2008; *Zhang et al.*, 2008).

In this paper we present observations from a four-way conjunction that occurred on 3 May 2007 between the THEMIS, Cluster and Double Star TC-1 satellites and the SuperDARN ionospheric radars. During the interval 10:00 to 15:00 UT reconnection took place at the dayside magnetopause and FTE structures were generated for several hours. THEMIS and Cluster, situated on the equatorial flank and high-latitude Southern Hemisphere magnetopause respectively, both observed FTEs throughout the five hour interval. THEMIS was aligned in a string broadly along the direction of motion of the FTEs, which allows the motion of the FTEs to be tracked along 17,000 km and the acceleration to be measured. TC-1 was situated nearer local noon (but at mid-latitudes) and observed only one FTE, indicating that reconnection was less variable there than at the reconnection site responsible for the signatures observed by THEMIS and Cluster.

In the following section, we introduce the instrumentation used in this paper. This is followed by an outline of the in situ and ionospheric observations, and in Section 4 we discuss the implications for the acceleration of FTEs and the extent of the reconnection line.

2 Instrumentation

We present magnetopause observations from three spacecraft missions: the five-spacecraft THEMIS constellation (*Angelopoulos*, 2008), the four-spacecraft Cluster constellation (*Escoubet et al.*, 2001), and the Double Star TC-1 satellite (*Liu et al.*, 2005). The ionospheric response to magnetopause activity is shown using data from the Super Dual Auroral Radar Network (SuperDARN) array of high-latitude radars (*Greenwald et al.*, 1995; *Chisham et al.*, 2007). The upstream conditions are provided by the OMNI High Resolution database, which consists of Wind observations (*Lepping et al.*, 1995) which have been lagged to the magnetopause using a time-varying lag (*King and Papitashvili*, 2005).

2.1 THEMIS

The locations of the spacecraft near the magnetopause are shown in the top row of Figure 1. In May 2007, the THEMIS spacecraft were in the 'coast phase' of the mission, during which the five spacecraft formed a string, all following the same orbit. Between 11:00 and 15:00 UT on 3 May, the spacecraft crossed the post-noon magnetopause from the magnetosphere into the magnetosheath at low latitudes. In this paper, we primarily use magnetic field data from the Fluxgate Magnetometer instrument (FGM: *Auster et al.*, 2008). Between 11:00 and 13:14 UT, THEMIS was in its fast survey mode, and magnetic field data were available at 4 Hz cadence. Thereafter, the spacecraft were in a slow survey mode and the magnetic field data were only available at spin resolution (∼3 s). Data at both resolutions are employed in this paper. We also show spin resolution electron spectrograms and quote lower-resolution ion moments from the Electrostatic Analyzer (ESA: *McFadden et al.*, 2008).

2.2 Cluster and Double Star

The Cluster spacecraft were situated in the magnetosheath near the dawn terminator and in the Southern Hemisphere. In this paper, we show magnetic field data at 5 Hz and spin (∼4 s) resolution from the Cluster FGM instrument (*Balogh et al.*, 2001) and spin resolution electron spectrograms from the Plasma Electron and Current Experiment (PEACE: *Johnstone et al.*, 1997).

The Double Star TC-1 satellite was near the magnetopause near local noon and in the Southern Hemisphere. Magnetic field data are provided at spin (∼4 s) resolution from the Fluxgate Magnetometer (*Carr et al.*, 2005). Electron data are provided by the Double Star PEACE instrument (*Fazakerley et al.*, 2005), which was in a mode that returned three-dimensional distributions every spin. The energy range of the instrument was sampled over two spins, so each pair of distributions has been combined resulting in a resolution of ∼8 s. The distributions were then binned to pitch angles, which are shown in this paper. Ion moment parameters are provided by the TC-1 HIA instrument (*Rème et al.*, 2005), which are also available at spin resolution.

2.3 SuperDARN

Four Northern Hemisphere radars are used: Þykvibær, Stokkseyri, Goose Bay and Kapuskasing. The locations and fields of view of these radars are shown in the bottom row of Figure 1. Each panel shows a polar grid of magnetic latitude (MLAT) and magnetic local time (MLT). As described by *Milan et al.* (1997), each radar transmits high frequency radio waves, which are scattered from ionospheric electron density irregularities that move as part of the ionospheric convection process. When backscatter is observed, the ionospheric convection velocity and the backscatter power and spectral width are measured. Data points with a low velocity and low spectral width are flagged as ground scatter. A sweep of each field of view is performed every two minutes. The fields of view of these radars were biased towards the pre-noon sector at 11:00 UT (except for Þykvibær), but had rotated to provide coverage of the pre- and post-noon sectors by 15:00 UT.

3 Observations

3.1 Solar wind conditions

The lagged solar wind conditions are given in Figure 2, which shows the GSM components and magnitude of the IMF observed by the Wind spacecraft, the IMF clock angle ($\theta_{CA} = \arctan[B_Y/B_Z]$), the solar wind density, radial velocity component and dynamic pressure, all from the OMNI database. Throughout the interval, the IMF was dominated by the B_Y component, which was consistently directed dawnward. The B_Z component was initially southward although there were some brief northward excursions in the first half of the interval, and after 13:00 UT the IMF turned northward (but was still predominantly dawnward). After 14:30 UT, the B_Z component observed by Wind increased as B_Y dropped to near-zero. Figure 2 also shows the clock angle of the magnetic fields observed by Cluster 3 and THEMIS-C, which were situated in the magnetosheath. The clock angles observed by Wind and Cluster compare relatively well, except for the northward excursion observed by Wind after 14:30 UT. This excursion was not observed by Cluster, although it was evident at THEMIS after 14:40 UT.

3.2 Ionospheric observations

Figure 3 summarises the ionospheric observations made by the SuperDARN radars. Figures 3(a-d) show spatial views of the ionospheric velocity deduced from the radar backscatter at 10:40 and 13:30 UT as observed by the Þykvibær, Stokkseyri, Goose Bay and Kapuskasing radars. Figures 3(a) and (c) show the data from Þykvibær and Stokkseyri at 10:40 and 13:30 UT respectively, whilst Figures 3(b) and (d) show the data from Goose Bay and Kapuskasing at the same times. Each panel shows the same polar grid of magnetic latitude and magnetic local time as is used in Figure 1. They also show the Northern Hemisphere footprints of THEMIS-E and TC-1 (the footprint of TC-1 in Figures 3(a) and (b) is calculated from the position of TC-1 shortly after its magnetopause crossing into the magnetosphere at 11:30 UT). Cluster 3 was in the magnetosheath throughout the interval; when it subsequently crossed into the magnetosphere at 16:10 UT, it entered onto Southern Hemisphere lobe field lines, and therefore did not have a footprint in the Northern Hemisphere. The Southern Hemisphere footprint of these field lines was at 10h MLT; this magnetic local time is indicated by a thick dashed line in Figure 3(a-d) for illustrative purposes.

Figures 3(e-h) show time series of the ionospheric velocity as a function of magnetic latitude for Þykvibær, Stokkseyri, Goose Bay and Kapuskasing, and (i-l) show the backscatter power for the same radars and in the same format. Each panel shows the data from one radar beam. The beams selected for Þykvibær and Stokkseyri are the most northward-pointing beams. The beams selected for Goose Bay and Kapuskasing are those which contained the most backscatter. All four selected beams have an azimuthal component in their lines of sight. Each selected beam is marked in Figures 3(a-d).

Þykvibær observed a burst of strong poleward flow in the near-noon MLT sector between 10:36 and 10:48 UT between 79° and 82° MLAT, indicative of a burst of reconnection at the near-noon magnetopause (Figures 3a & e). After 10:48 UT, very little was observed in the noon sector apart from ground scatter (shaded gray). The lack of ionospheric scatter after 10:48 UT means that it is not possible to conclude whether or not the reconnection burst continued at the near-noon magnetopause.

The Kapuskasing radar observed fast flows away from the radar (poleward and/or duskward) throughout the interval from 10:00 to 15:00 UT (Figure 3h). As time progressed, the backscatter was observed at gradually higher magnetic latitudes. However, this may be a local time effect rather than indicating the migration of the open/closed field line boundary to higher latitudes. Between 10:00 UT and 15:00 UT, the fast flows were observed between ∼6h and 11h MLT as the field of view of the radar rotated in local time. At 12:00 UT, the radio frequencies used by the Kapuskasing and Goose Bay radars changed. Consequently, the backscatter power decreased temporarily at Kapuskasing, but strong and persistent flows were observed by Goose Bay (at 82° MLAT and 10h MLT). Some structure is visible in the backscatter power (Figures 3k & l) which indicates the propagation of regions of high backscatter power to higher magnetic latitudes. Such features are referred to as Poleward Moving Radar Auroral Forms (PMRAFs: *Milan et al.*, 2000; *Wild et al.*, 2001), and indicate the occurrence of time-varying reconnection at the magnetopause in this local time sector. At their largest extent (13:00 UT onwards), PMRAFs were observed by both Goose Bay and Kapuskasing, between 7h and 14h MLT, as shown in Figure 3(d).

The more northerly beams of the Stokkseyri radar observed a long-lasting patch of radar backscatter

between 78 and 81° MLAT (Figure 3f). The field of view of Stokkseyri overlaps with that of Goose Bay, and both radars observed backscatter from the same region of the ionosphere. The flows observed at Stokkseyri were weaker than those observed at Goose Bay, indicating that the bulk of the ionospheric flow was perpendicular to the Stokkseyri beam directions. However, there was a clear, repeated variation between flows with components towards the Stokkseyri radar (equatorward and/or duskward) and away from the radar (poleward and/or dawnward), and there was also modulation in the backscatter power (Figure 3j). Observed ionospheric velocity components along the line of sight of the Stokkseyri radar were typically of order ±200 km s^{-1}, but some flow bursts directed away from the radar peaked at velocity components of 400 km s^{-1}. These pulsed flows were observed between 10:00 and 14:00 UT, and correspond to the same region of the ionosphere as is observed by the Goose Bay radar, suggesting that the lack of fast flows observed by Goose Bay before 12:00 UT is due to the sounding frequency used by Goose Bay.

The line-of-sight velocities in Figure 3 can be combined with the "map potential" model of ionospheric flow to derive two-dimensional velocities (*Ruohoniemi and Baker*, 1998). The line-of-sight velocities are mapped onto a polar grid, and then fitted to an expansion of the electrostatic potential in spherical harmonics, which is stabilised by a statistical model in regions where there are no observations. This analysis is shown for half-hourly snapshots in Figure 4, which shows the brief burst of near-noon poleward flow observed at 10:40 UT (Figure 4b). The fast flows observed by the Goose Bay and Kapuskasing radars start near local dawn in panel (c), are visible near local noon in panel (e), become enhanced in panels (g-i) and decay in panels (j-l).

3.3 Magnetopause observations

The orientation and separations of the THEMIS and Cluster spacecraft at 13:00 UT are shown in boundary normal coordinates (*Russell and Elphic*, 1978) in Figure 5, and an overview of the magnetic field & electron observations made by these spacecraft is shown in Figure 6. The string of THEMIS spacecraft was led by TH-C, followed by TH-B, D, A and E. At 13:00 UT, TH-C and TH-E were separated by 4,600 km in the direction normal to the magnetopause, and 21,600 km tangential to the magnetopause. Between 11:05 and 12:02 UT, all five spacecraft were situated in the magnetosphere, observing a hot, rare electron plasma and a magnetic field dominated by the strongly positive B_L component. At 12:02 UT, TH-C crossed the magnetopause into the magnetosheath where it observed: a cooler, denser plasma; a weaker, generally negative B_L component and a positive B_M component. The THEMIS string then straddled the magnetopause until TH-E crossed into the magnetosheath at 14:35 UT, at which point the magnetosheath magnetic field was positive in both the B_L and B_M components (corresponding to the northward turning of the IMF observed at 14:30 UT). The Cluster spacecraft were oriented in an elongated triangle, since Clusters 3 and 4 were only separated by 700 km, where the three sides of the triangle (C3–C1, C1–C2, C2–C3) were 7900 km, 3200 km and 6500 km. All four spacecraft were situated in the magnetosheath throughout the interval.

The boundary normal coordinates were derived independently for THEMIS and Cluster. For THEMIS, the normal was determined by applying minimum variance analysis (MVA: *Sonnerup and Cahill*, 1967; *Sonnerup and Scheible*, 1998) to the 4 Hz magnetic field data from TH-D as the spacecraft crossed the magnetopause between 12:08:00 and 12:08:40 UT ($\lambda_{int}/\lambda_{min} = 4.52$). The corresponding minimum variance eigenvector was taken to be the magnetopause normal ($\hat{\mathbf{n}} = (0.842, 0.530, -0.099)_{GSE}$). The vector $\hat{\mathbf{l}} = (0.120, -0.006, 0.993)_{GSE}$ was derived by projecting the Earth's magnetic dipole onto the plane defined by $\hat{\mathbf{n}}$, and $\hat{\mathbf{m}} = \hat{\mathbf{n}} \times \hat{\mathbf{l}} = (0.525, -0.848, -0.069)_{GSE}$ completes the set. $\hat{\mathbf{n}}$ is directed largely dawnward, and $\hat{\mathbf{l}}$ is predominantly in the $\hat{\mathbf{z}}_{GSE}$ direction, consistent with the low-latitude, post-noon location of the spacecraft.

Since Cluster did not cross the magnetopause in this interval (Figure 6), the rotation matrix to boundary normal coordinates was determined from the *Roelof and Sibeck* (1993) magnetopause model: $\hat{\mathbf{n}} = (0.519, -0.599, -0.609)_{GSE}$, $\hat{\mathbf{l}} = (0.486, -0.379, 0.787)_{GSE}$ and $\hat{\mathbf{m}} = (-0.703, -0.705, 0.095)_{GSE}$.

3.3.1 THEMIS

FTEs can be identified from their characteristic bipolar B_N signatures throughout the interval 11:00 to 15:00 UT in Figure 6. Some enlargements of the B_N traces are provided in Figure 7, which shows B_N

traces for the whole interval in four one-hour panels. Each panel shows a trace from a different spacecraft, and for a different one-hour block from 11:00 through to 15:00 UT. FTEs were first observed at 11:00 UT by TH-C, the outermost spacecraft and therefore the nearest to the magnetopause (Figure 7a). At this time, the THEMIS spacecraft were all in the magnetosphere, identified by the positive B_L components in Figure 6. At the same time, the other THEMIS spacecraft observed lower-frequency Pc5 oscillations in the B_N component (Figure 6). The Pc5 variations persisted at TH-A, B and D until 12:00 UT, when these three spacecraft started to observe FTEs (e.g. TH-B, Figure 7b). At the same time, TH-C crossed the magnetopause into the magnetosheath. Between 13:00 and 14:00 UT TH-B and TH-D crossed the magnetopause several times (Figure 6) and FTEs continued to be observed by these spacecraft (e.g. Figure 7c). By 14:00 UT, TH-E was close enough to the magnetopause that it was able to observe FTEs (Figure 7d), and shortly after 14:30 UT two FTEs were observed by all five THEMIS spacecraft simultaneously (Figure 8).

The observation of two FTEs by all five THEMIS spacecraft allows us to carry out multi-spacecraft timing analysis (*Russell et al.*, 1983; *Harvey*, 1998) to investigate the velocities of the FTEs. At 14:38 UT, the spacecraft were aligned in a string roughly tangential to the magnetopause. The maximum spacecraft separation was approximately 17,700 km in the $\hat{\mathbf{m}}$ direction, 4,800 km in the $\hat{\mathbf{l}}$ direction and 2,200 km normal to the magnetopause. The normal separation was less than the typical scale size of an FTE normal to the magnetopause as determined by *Saunders et al.* (1984). Since the spacecraft were aligned in a string, it is only possible to derive the component of velocity in the dimension along the string, which is largely the $\hat{\mathbf{m}}$ direction. However, as there are five spacecraft it is possible to assess whether this velocity component is constant as the FTE moves downtail.

The time between each FTE being observed at TH-A (taken to be the reference spacecraft) and each of the other spacecraft is plotted against the distance of each spacecraft from TH-A in Figure 9. The time between the FTE being observed at each spacecraft was determined by identifying the mid-point of each B_N signature (indicated in Figure 8 by vertical gray lines), and the error bars reflect the variation which would be introduced by aligning the positive or negative peaks of the bipolar signature instead (e.g. *Fear et al.*, 2007). The minimum error assumed is the resolution of the data used for this analysis (3 s). The distance plotted is the separation of the spacecraft in the $\hat{\mathbf{l}}$-$\hat{\mathbf{m}}$ plane. The timing uncertainties are larger for the second FTE than the first, due to the fact that the B_N signatures are less clear (Figure 8).

The solid line in each panel of Figure 9 is a linear best fit line of the form $s=s_0 + vt$. Here, s is the displacement of the FTE, v is the component of the FTE velocity along the spacecraft string, t is time and s_0 is the displacement at t=0 (which should be zero as the displacement and time are defined relative to TH-A). The gradients of the graphs are v=263 km s^{-1} and 189 km s^{-1} for the FTEs at 14:34 and 14:42 UT respectively, which correspond to the components of the FTE velocities along the THEMIS string. The offsets are s_0=-1064 km and +109 km, which are small compared with the spacecraft separations. These speeds are typical of those that have been observed by Cluster (see Figure 6c of *Fear et al.*, 2007).

The hatched line in each panel is a quadratic best fit, of the form $s=s_0 + vt + \frac{1}{2}at^2$. This introduces an acceleration, a, to the fitting process. The best fit velocity components (at TH-A) are v=301 km s^{-1} and 185 km s^{-1} respectively, the offsets are s_0=-1153 km and +88 km, and the acceleration terms are a=-1.4 km s^{-2} and +0.12 km s^{-2} (therefore the hatched line for the 14:42 UT FTE is barely distinguishable from the solid line).

The acceleration terms are small, and we conclude that these are negligible on the separation scale of the THEMIS spacecraft. In fact, the acceleration term for the 14:42 UT FTE represents a slight acceleration, whilst the term for the 14:34 UT FTE represents a small deceleration. Since the separation of the THEMIS spacecraft is significantly greater than the maximum proposed separation of the Cluster spacecraft for the entire lifetime of that mission, we can conclude that the assumption of constant velocity used in multi-spacecraft timing is reasonable, at least on the magnetopause flanks.

3.3.2 Cluster

The magnetic field observed by Cluster is also shown in boundary normal coordinates in Figure 6. Throughout the interval, the Cluster spacecraft were situated in the magnetosheath, and moved towards the magnetopause and Southern Hemisphere cusp. Reverse polarity FTEs were observed by all four

spacecraft throughout the interval; the magnetic field signatures were initially weak (Figure 10), but became gradually stronger as the spacecraft approached the magnetopause (Figure 6).

The observation of standard polarity FTEs at THEMIS and reverse polarity FTEs at Cluster for the entire interval from 11:00 to 15:00 UT demonstrates that reconnection was occurring at the dayside magnetopause throughout this period, as also evident from the SuperDARN observations (Figure 3).

3.3.3 Double Star

TC-1 was located in the magnetosheath at 11:00 UT (Figure 11), and crossed the magnetopause between 11:32 and 11:34 UT into the magnetosphere. The magnetopause normal was determined from minimum variance analysis over the interval 11:30 to 11:36 UT; the tangential vectors were determined using the same procedure as for THEMIS: $\hat{\mathbf{n}}$ = (0.748, 0.434, -0.502)$_{GSE}$, $\hat{\mathbf{l}}$ = (0.457, 0.211, 0.864)$_{GSE}$ and $\hat{\mathbf{m}}$ = (0.481, -0.976, -0.040)$_{GSE}$.

Figure 11 shows the electron, magnetic field and ion observations made by the Double Star TC-1 satellite between 11:00 and 12:30 UT. The figure shows, from top, electron spectrograms for pitch angles parallel, perpendicular and antiparallel to the magnetic field; the magnetic field in boundary normal coordinates and the ion density and velocity (also in boundary normal coordinates). Electron data are full three-dimensional distributions which have been binned to pitch angles. The spacecraft was initially in the magnetosheath (evidenced by the cool, dense, isotropic electron distribution and large ion densities), where it observed a southward- and dawnward-directed magnetic field ($B_L < 0$, $B_M > 0$). At 11:33 UT, TC-1 crossed the magnetopause, after which it observed a northward magnetic field ($B_L > 0$) and generally a hotter, rarer plasma distribution. There is some evidence for boundary layer structure shortly after the magnetopause crossing, corresponding to two brief reductions in the B_L component, which remained positive, at 11:36 and 11:39 UT. At these times, the electron spectrum changed to one that was more magnetosheath-like but with lower fluxes. The spacecraft then remained in the magnetosphere until 12:00 UT, when it re-entered the magnetosheath for fifteen minutes, and then re-entered the magnetosphere. Between 11:30 and 11:50 UT, the ion bulk velocity was highly variable, with peaks in magnitude that were greater than the magnetosheath bulk speed.

During this entire 90 minute period, during which the spacecraft was near the magnetopause, only one clear flux transfer event was observed (a reverse polarity FTE at 11:13 UT – highlighted by red lines in Figure 11). Figure 12 shows an enlargement of the electron and magnetic field data and the bulk ion speed for the 25 minute period around the magnetopause crossing at 11:33 UT. Just before the magnetopause crossing, the magnetosheath electron population appeared to be heated slightly (e.g. ∼11:29 UT). After the magnetopause crossing at 11:33 UT, a hotter, bidirectional, field-aligned electron distribution was observed, interrupted by two magnetosheath-like boundary layer entries and corresponding B_L reductions noted in the previous paragraph. High energy electrons with peak fluxes near 90° pitch angles, more typical of the magnetosphere-proper, were initially weak in flux but became clearer by ∼11:44 UT. The bidirectional field-aligned population was intermediate in energy between that of the 90° pitch angle magnetospheric population and the magnetosheath population.

The boundary layer structure observed by TC-1 and the observation of an FTE at 11:13 UT suggest that reconnection also occurred near the location of TC-1. To test this hypothesis, we carried out a series of Walén tests (*Walén*, 1944; *Sonnerup et al.*, 1987; *Khrabrov and Sonnerup*, 1998) on the ion velocities observed by TC-1 in a range of intervals about the magnetopause crossing time. Following the method of *Khrabrov and Sonnerup* (1998), we sought a so-called de Hoffmann-Teller frame with constant acceleration, in which the convection electric field ($\mathbf{E}_C = -\mathbf{v} \times \mathbf{B}$) transformed to zero (*de Hoffmann and Teller*, 1950). We found such a frame for the interval 11:33:07 to 11:33:32 UT (indicated by red lines in Figure 12). During this interval, there was a brief gap in the magnetometer data (see Figure 12), so the magnetic field data were interpolated where necessary. The velocity of the de Hoffmann-Teller frame was $\mathbf{V}_{HT} = \mathbf{V}_{HT0} + \mathbf{a}_{HT} \cdot t$, where $\mathbf{V}_{HT0}$ was (-171, 227, -138)$_{GSE}$ km s^{-1} and $\mathbf{a}_{HT}$ was (-4.15, -5.75, -8.27)$_{GSE}$ km s^{-2}. The normal components $\mathbf{V}_{HT0n}$ and $\mathbf{a}_{HTn}$ were 40 km s^{-1} and -1.5 km s^{-2} respectively, corresponding to an outward-moving frame (consistent with the magnetopause moving outward across the spacecraft as observed). Figure 13a is a scatter plot of the convection electric field of the plasma in the GSE frame ($\mathbf{E}_C$) against the electric field induced by the motion of the frame ($\mathbf{E}_{HT} = -\mathbf{V}_{HT} \times \mathbf{B}$). The points relying on the interpolated magnetic field are identified by circles. The correlation is good (0.996), giving confidence that this procedure has found the de Hoffmann-Teller

frame. If reconnection is ongoing and the magnetopause is therefore a rotational discontinuity, the Walén test should be satisfied: the velocity of the ions in the de Hoffmann-Teller frame should be equal to the Alfvén velocity ($\mathbf{V}_A = \mathbf{B}\sqrt{(1-\alpha)/\mu_0\rho}$, where ρ is the mass density, the pressure anisotropy α is $(p_\parallel - p_\perp)\mu_0/B^2$, and μ_0 is the permeability of free space). It is shown in Figure 13b that this is the case for some of the data points. Those points in black represent the velocities in the de Hoffmann-Teller frame observed during the first four spins, when the density was above 1.5 cm^{-3}, and all four points correspond well to the Alfvén velocity. Therefore the ion distributions with magnetosheath density but faster speeds correspond well to reconnection flows. The points in gray represent the following three spins, during which densities below 1.5 cm^{-3} were observed. Although these flows were indeed faster than the background magnetosheath velocity, they were slower than the calculated Alfvén velocity. However, it has been noted by *Paschmann and Sonnerup* (2008) that contrary to the MHD-based theoretical prediction, $\rho(1-\alpha)$ does not always remain constant within a rotational discontinuity. The reason for this discrepancy is not understood, but it has been found that the quality of the Walén test is often improved by replacing the observed plasma density by $\rho = \rho_1(1-\alpha_1)/(1-\alpha)$, where ρ_1 and α_1 are the mass density and anisotropy at a reference point upstream (*Paschmann et al.*, 1986; *Sonnerup et al.*, 1987; *Phan et al.*, 2004; *Retinò et al.*, 2005). The results of the Walén test using this substitution in the calculation of the Alfvén velocity is shown in Figure 13c. ρ_1 and α_1 refer to the parameters at 11:28 UT. The substitution has a significant effect on the Alfvén velocity in the low density region, and the Walén test is satisfied.

We therefore find evidence for the magnetopause being open in the vicinity of TC-1 at the time of the magnetopause crossing. Furthermore, the prior passage of an FTE and the fast flows observed by the Þykvibær radar at 10:40 UT, indicate that the magnetopause must also have been open nearby beforehand, and the observation of FTE signatures at THEMIS-C (Figure 7a) and Cluster (Figure 10) at the same time as the TC-1 magnetopause crossing indicates that reconnection continued elsewhere.

4 Discussion

We shall now seek to understand the above observations in terms of a simple model of reconnected field-line motion developed by *Cooling et al.* (2001) (hereinafter referred to as the Cooling model). This model is based on earlier work by *Cowley and Owen* (1989), who developed a simple expression for the velocity of a reconnected magnetic field line as a function of the local magnetosheath magnetic field, density and velocity, based on stress balance at the magnetopause. The Cooling model evaluates this velocity at any given position on the magnetopause based on upstream IMF input by using models by *Spreiter et al.* (1966) and *Kobel and Flückiger* (1994) to evaluate the magnetosheath density/speed and magnetic field. The model has been used by several authors to explain observed FTE motion (e.g. *Wild et al.*, 2005; *Dunlop et al.*, 2005; *Fear et al.*, 2005), and it has been tested in a statistical study by *Fear et al.* (2007).

Figure 14 shows the results of the model run, using IMF conditions from 11:13 UT, shortly before the TC-1 magnetopause crossing [$\mathbf{B}_{IMF}$ = (-2, -4, -1)$_{GSM}$ nT, n_{SW} = 6 cm^{-3}, V_{SW} = 335 km s^{-1}]. The figure represents a view of the magnetopause as seen from the Sun; dotted concentric circles represent contours in X_{GSM}. The Cooling model allows the user to specify an initial reconnection site, from which a component-reconnection X-line is traced for a user-specified length. The black line in the centre of the figure represents an X-line, which has been initiated at the subsolar point with an arbitrary length of 12 R_E. The length of the X-line has been selected to illustrate a scenario where reconnection signatures are observed at THEMIS, Cluster and TC-1. The solid and dashed lines emanating from the X-line are model flux tube paths for open magnetic field lines connected to the Northern and Southern Hemisphere respectively; the lines represent the progression of the points at which specific open field lines thread the magnetopause as time progresses (from a time t=0 to a time 600 s later), and pairs of paths have been initiated at 2 R_E intervals. As expected for a period of dawnward B_Y-dominated IMF, the flux tubes connected to the Northern Hemisphere move northward and duskward, whilst those connected to the Southern Hemisphere move southward and dawnward. Flux tubes connected to the Northern Hemisphere move predominantly northward at the dawnward end of the X-line, and duskward at the dusk end; similarly flux tubes connected to the Southern Hemisphere moved predominantly southward/dawnward at the duskward/dawnward ends.

Flux tubes that are opened at the X-line in Figure 14 move past both the THEMIS and Cluster

spacecraft. The model flux tubes that move past Cluster are connected to the Southern Hemisphere, consistent with the observation of heated electrons moving parallel to the magnetic field (visible after 13:00 UT in Figure 6) whilst those moving past THEMIS are connected to the Northern Hemisphere. Since the solar wind conditions are largely stable, similar model results are obtained using other solar wind inputs from the rest of the interval up to 14:30 UT, when the IMF turned strongly northward (although the strong northward turn was not observed by THEMIS until after 14:40 UT). Using the lagged IMF observed at 14:35 UT [$\mathbf{B}_{IMF}$ = (1.4,-1.9,4.1)$_{GSM}$ nT], the model FTE velocity at the location of TH-A is (-125,-200,-60)$_{LMN}$ km s^{-1}, and the component along the THEMIS string is 226 km s^{-1}. Whilst the lagged IMF at this time is strongly northward and does not favor dayside reconnection, we note that this was during the interval between the strong northward rotation being observed in the lagged IMF data and at THEMIS. The magnetosheath clock angle observed by THEMIS was nearer to 65°/70° and therefore more favorable for dayside reconnection. Furthermore, the model FTE velocity is dominated by the magnetosheath velocity at this point (using an IMF of (-0.5,-4.2,1.3)$_{GSM}$ nT results in an FTE velocity of (-73,-227,-63)$_{LMN}$ km s^{-1}, and a component along the string of 238 km s^{-1}). This speed compares well with the speeds calculated in Section 3.3.1 for the two FTEs which were observed by all five THEMIS spacecraft. It is indicated in Figure 9 by a dashed line in both panels which passes through the origin (representing TH-A) and which has a gradient of 226 km s^{-1}. The dashed line is very similar to the best fit line for the FTE observed at 14:34 UT, but is somewhat steeper than the best fit line for the 14:42 UT FTE. Nevertheless, the Cooling model velocity is still consistent with the delay times between the FTE signatures being observed at almost all of the spacecraft within the stated error bars. The acceleration of the model flux tubes at the location of THEMIS is ∼0.4 km s^{-2}, which is similar in magnitude to the acceleration values determined from Figure 9. However, this is clearly small compared with the uncertainties in the observational determination of the acceleration, since the difference between the two values obtained observationally was of the same order as the values themselves.

Snapshots of the plasma moments were available from TH-C, D and E every few minutes. At around this time, the magnetosheath velocity observed by TH-D was (-30,-130,-30)$_{LMN}$ km s^{-1}; the component of this velocity along the projection of the spacecraft string onto the magnetopause was ∼130 km s^{-1}. Therefore both FTEs appeared to be moving faster than the background magnetosheath flow, as a result of the magnetic tension acting on the FTE (which is incorporated into the Cooling model). The model magnetosheath velocity at TH-D was (-43,-187,-55)$_{LMN}$ km s^{-1} (191 km s^{-1} along the string). The discrepancy of 60 km s^{-1} between the observed and modelled magnetosheath speeds is one factor in the 37 km s^{-1} model overestimation of the observed velocity component of the 14:42 UT FTE, although the model FTE velocity was a slight underestimate for the 14:34 UT FTE.

The speeds quoted above (both those derived from observations and from the Cooling model) are estimates for the components of the FTE velocity along the spacecraft string. Since the THEMIS spacecraft were aligned in the azimuthal ($\hat{\mathbf{m}}$) direction, this corresponds broadly to the tailward components of the FTE velocities. Since the spacecraft were aligned in a string, we cannot derive the three-dimensional velocity from multi-spacecraft methods, but we note that the 3D Cooling model velocity was only 22° from the projection of the spacecraft string onto the magnetopause surface, therefore it is likely that the velocity components calculated from the observations are very similar to the total FTE speeds.

We can compare this direction of the model velocity vector with single-spacecraft estimates of the FTE axial orientation; one way to estimate the FTE axis is by applying minimum variance analysis to the FTE signature. *Xiao et al.* (2004) examined the application of MVA to magnetic field data in modelled flux ropes, and found that the eigenvector corresponding to the axis depended critically on the path of the spacecraft relative to the flux rope and on the model of flux rope assumed. They found that if their modelled spacecraft path crossed only the region of draped magnetic field around the flux tube (as previously modelled by *Farrugia et al.*, 1987), the axial direction was indicated by the minimum variance direction since in the assumption of incompressible flow made by *Farrugia et al.* the magnetic field line was not deflected in the axial direction. If the modelled spacecraft cut through a force-free flux rope, the intermediate variance direction indicated the axial direction reasonably well, and if the spacecraft cut through a flux rope with a strong core field, then either the maximum or intermediate eigenvectors approximated the axis (depending on the proximity of the spacecraft pass to the center of the flux rope). Therefore interpretation of MVA results on FTE signatures must be treated with caution.

None of the spacecraft observed a strong core field during either FTE (Figure 8). We can determine whether the spacecraft entered onto the reconnected 'core' of the FTEs by examining the electron spectrograms for each spacecraft, which are available from TH-C, D and E and are shown in Figure 8.

TH-C and D were situated in the magnetosheath, and observed no significant change in the electron distribution during the passage of either FTE. Therefore these spacecraft only observed the region of draped flux around the FTE core. (A slight heating was observed in the ions, not shown, but this may be a remote sensing effect as the spacecraft moved closer to open field lines and were therefore able to observe heated ions due to their larger gyroradii). TH-E observed the 14:34 UT FTE as it crossed the magnetopause, and therefore it is likely that TH-E entered onto open magnetic field lines although there is no sign that the magnetosheath plasma observed during the FTE has been heated. TH-E observed a slight increase in the flux of hot electrons (∼300-1000 eV) during the passage of the 14:42 UT FTE. No plasma observations were available from TH-A or B, but by this time both spacecraft were located further out into the magnetosheath than TH-C, so the absence of reconnection signatures at TH-C suggests that TH-A and B both only observed the field line draping around the FTEs.

The results of MVA on the magnetic signatures of both FTEs are shown in Table 1. The minimum and intermediate variance eigenvectors were not very well defined in any of the cases (the ratios of the intermediate to minimum variance eigenvalues ranged between 1.66 and 2.20 for the first FTE), which is in part due to the small number of FGM data points during each FTE passage, since high resolution data were not available after 13:14 UT. It is therefore likely that in some cases the MVA technique fails to recover the axial direction. However, four of the five minimum variance eigenvectors were aligned within ∼25° of $\hat{\mathbf{l}}$ (the exception being TH-C). Since it appears likely that TH-E observed open magnetic field lines, it is surprising that the minimum variance eigenvector is similar to three of the other four vectors. One would expect the intermediate variance eigenvector, $(0.092, 0.991, 0.093)_{LMN}$ to indicate the axial direction if TH-E did make a crossing of the flux tube (the eigenvalue ratio $\lambda_{max}/\lambda_{int}$ was 2.11). For the second FTE there was more variation, but we note that the magnetic field signatures observed by TH-B, C and D were weak (Figure 8), and the minimum variance eigenvalue for TH-E was particularly poorly defined ($\lambda_{int}/\lambda_{min} = 1.3$). The minimum variance eigenvector for TH-A was again close to $\hat{\mathbf{l}}$. To summarize, MVA results from TH-A (both FTEs) and TH-B & D (14:34 UT) indicate that the axial direction is likely to be close to $\hat{\mathbf{l}}$, whilst the results from TH-C and E (14:34 UT) suggest it may have a stronger component in the $\hat{\mathbf{m}}$ and/or $\hat{\mathbf{n}}$ directions. Recalling again that the eigenvalue ratios indicate that the eigenvectors are not well defined in any of the cases, we conclude on the balance of probabilities that the FTE axes were most likely aligned to within ∼25° of $\hat{\mathbf{l}}$, and therefore largely perpendicular to the string of spacecraft.

Although TC-1 was not in the vicinity of the magnetopause for as long as Cluster and THEMIS, it did cross the magnetopause three times (Figure 11), much nearer to the subsolar point than THEMIS or Cluster (Figures 1 and 14). However, TC-1 observed only one flux transfer event in the ∼90 minute period in which the spacecraft was near the magnetopause.

There are two possible reasons for the lack of FTE signatures observed by TC-1. The first is that reconnection was not as active, or not as variable, near TC-1 at the time of the magnetopause crossing as it was at the part(s) of the X-line which gave rise to the signatures observed by THEMIS and Cluster. The second possible explanation, suggested by *Russell et al.* (1985) and also discussed by *Southwood et al.* (1986), is that whilst reconnection may be occurring nearby, the spacecraft may be so close to the X-line that the FTE structures are in an early stage of their development and therefore not easily recognisable from the classical signatures. Indeed, *Wang et al.* (2005) showed a correlation between the peak-to-peak magnitude of the bipolar B_N signature and magnetic latitude, although their survey did not sample the subsolar region. However, if the FTE signature observed by TC-1 at 11:13 UT was formed at the same reconnection line as gave rise to the fast flows at the later magnetopause crossing, the observation of a clearly-defined FTE structure shows that there is indeed time for an FTE to form and be observed by TC-1. We also note that whilst *Russell et al.* (1985) and *Southwood et al.* (1986) discussed a lack of FTE observations near the subsolar point, no subsequent surveys of low-latitude FTE signatures have found such a gap (e.g. *Kawano and Russell*, 1996).

The Cooling model run suggests that the FTE signatures observed by THEMIS and Cluster can be explained by a relatively narrow extent of X-line near the subsolar point (Figure 14). The subsequent paths of flux tubes opened at the subsolar X-line fan out such that they move past both spacecraft constellations, so the model flux tubes observed by both THEMIS and Cluster can be traced back to within 2 R_E of the subsolar point. TC-1 was located nearer the subsolar, tilted reconnection line assumed in the Cooling model, but 7 R_E from the subsolar point. Since reconnection signatures were observed by TC-1 (and at its footprint in the Þykvibær radar field of view), this suggests that the X-line extends

at least 7 R_E from the subsolar point, and that the open flux tubes observed by TC-1 were reconnected nearer to the spacecraft (at a different part of the X-line from the open flux observed by THEMIS and Cluster). Therefore the modulation of the reconnection process appears to be different at this location compared with nearer the subsolar point at the time of the TC-1 magnetopause crossing (if indeed the X-line is a single uniform structure).

5 Conclusions

We have presented observations from a five-hour interval on 3 May 2007, throughout which signatures of time-varying reconnection were observed by the THEMIS and Cluster spacecraft and some of the SuperDARN ionospheric radars. Cluster was situated in the high-latitude, pre-noon magnetosheath, and THEMIS was at the post-noon equatorial magnetopause. THEMIS and Cluster observed flux transfer event signatures throughout the interval (standard and reverse polarity respectively), which can be traced back using a model to within ∼2 R_E of the subsolar point. TC-1 crossed the magnetopause approximately 7 R_E from the subsolar point, and was near the magnetopause for approximately 90 minutes. During this time, TC-1 only observed a single (reverse polarity) flux transfer event. A Walén test was carried out on the ion velocity data from the magnetopause crossing, which showed that the enhanced ion velocities were consistent with those expected from ongoing reconnection. Therefore the reconnection line extended by at least 2 R_E from the subsolar point into the post-noon sector throughout the period 11:00-15:00 UT, and at the time of the TC-1 magnetopause crossing extended to at least 7 R_E from the subsolar point. Ionospheric observations suggest that the X-line covered several hours of local time in the pre-noon sector, but the different rates of FTE occurrence observed TC-1 and THEMIS/Cluster suggest that the variation in the reconnection rate differed between the subsolar point and the location of TC-1.

The observation of two flux transfer events by all five of the THEMIS spacecraft allowed the motion of the structures to be tracked for over a minute. It was found that, consistent with the predictions of the Cooling model, the acceleration of the FTEs was small (less than 1 km s^{-2}), demonstrating that determination of FTE velocities from multi-spacecraft timing techniques is reliable.

Acknowledgments

We acknowledge NASA contract NAS5-02099 and V. Angelopoulos for use of data from the THEMIS Mission, and specifically K.-H. Glaßmeier, U. Auster and W. Baumjohann for the use of THEMIS FGM data provided under the lead of the Technical University of Braunschweig and with financial support through the German Ministry for Economy and Technology and the German Center for Aviation and Space (DLR) under contract 50 OC 0302, and C. W. Carlson and J. P. McFadden for use of ESA data. We are similarly grateful to E. A. Lucek and the Cluster Active Archive for provision of Cluster FGM data. OMNI data were obtained from the GSFC/SPDF OMNIWeb interface at http://omniweb.gsfc.nasa.gov, and based upon Wind MFI and SWE observations courtesy of R. Lepping and K. Ogilvie. Work at the University of Leicester was supported by STFC grant PP/E000983/1. Some data analysis was done with the QSAS science analysis system provided by the United Kingdom Cluster Science Centre (Imperial College London and Queen Mary, University of London) supported by the Science and Technology Facilities Council (STFC).

References

Amm, O., E. F. Donovan, H. Frey, M. Lester, R. Nakamura, J. A. Wild, A. Aikio, M. Dunlop, K. Kauristie, A. Marchaudon, I. W. McCrea, H.-J. Opgenoorth, and A. Strømme (2005), Coordinated studies of the geospace environment using Cluster, satellite and ground-based data: an interim review, *Ann. Geophys.*, *23*, 2129–2170.

Angelopoulos, V. (2008), The THEMIS mission, *Space Sci. Rev.*, *141*, 5–34, doi:10.1007/s11214-008-9336-1.

Auster, H. U., K. H. Glassmeier, W. Magnes, O. Aydogar, W. Baumjohann, D. Constantinescu, D. Fischer, K. H. Fornacon, E. Georgescu, P. Harvey, O. Hillenmaier, R. Kroth, M. Ludlam, Y. Narita, R. Nakamura, K. Okrafka, F. Plaschke, I. Richter, H. Schwarzi, B. Stoll, A. Valavanoglou, and M. Wiedemann (2008), The THEMIS fluxgate magnetometer, *Space Sci. Rev.*, *141*, 235–264, doi: 10.1007/s11214-008-9365-9.

Balogh, A., C. M. Carr, M. H. Acuña, M. W. Dunlop, T. J. Beek, P. Brown, K.-H. Fornaçon, E. Georgescu, K.-H. Glassmeier, J. Harris, G. Musmann, T. Oddy, and K. Schwingenschuh (2001), The Cluster Magnetic Field Investigation: Overview of in-flight performance and initial results, *Ann. Geophys.*, *19*, 1207–1217.

Berchem, J., and C. T. Russell (1984), Flux transfer events on the magnetopause - spatial distribution and controlling factors, *J. Geophys. Res.*, *89*, 6689–6703.

Carr, C., P. Brown, T. L. Zhang, J. Gloag, T. Horbury, E. Lucek, W. Magnes, H. O'Brien, T. Oddy, U. Auster, P. Austin, O. Aydogar, A. Balogh, W. Baumjohann, T. Beek, H. Eichelberger, K.-H. Fornacon, E. Georgescu, K.-H. Glassmeier, M. Ludlam, R. Nakamura, and I. Richter (2005), The Double Star magnetic field investigation: instrument design, performance and highlights of the first year's observations, *Ann. Geophys.*, *23*, 2713–2732.

Chisham, G., M. Lester, S. E. Milan, M. P. Freeman, W. A. Bristow, A. Grocott, K. A. McWilliams, J. M. Ruohoniemi, T. K. Yeoman, P. L. Dyson, R. A. Greenwald, T. Kikuchi, M. Pinnock, J. P. S. Rash, N. Sato, G. J. Sofko, J.-P. Villain, and A. D. M. Walker (2007), A decade of the Super Dual Auroral Radar Network (SuperDARN): scientific achievements, new techniques and future directions, *Surv. Geophys.*, *28*, 33–109, doi:10.1007/s10712-007-9017-8.

Cooling, B. M. A., C. J. Owen, and S. J. Schwartz (2001), Role of the magnetosheath flow in determining the motion of open flux tubes, *J. Geophys. Res.*, *106*(A9), 18,763–18,776.

Cowley, S. W. H., and C. J. Owen (1989), A simple illustrative model of open flux tube motion over the dayside magnetopause, *Planet. Space Sci.*, *37*, 1461–1475.

Daly, P. W., D. J. Williams, C. T. Russell, and E. Keppler (1981), Particle signature of magnetic flux transfer events at the magnetopause, *J. Geophys. Res.*, *86*, 1628–1632.

Daly, P. W., R. P. Rijnbeek, N. Sckopke, C. T. Russell, and M. A. Saunders (1984), The distribution of reconnection geometry in flux transfer events using energetic ion, plasma and magnetic data, *J. Geophys. Res.*, *89*(A6), 3843–3854.

Dungey, J. W. (1961), Interplanetary magnetic field and the auroral zones, *Phys. Rev. Lett.*, *6*, 47–48, doi:10.1103/PhysRevLett.6.47.

Dungey, J. W. (1963), The structure of the exosphere or adventures in velocity space, in *The Earth's Environment*, edited by C. DeWitt, J. Hieblot, and A. Lebeau, pp. 505–550, Gordon and Breach, New York.

Dunlop, M. W., M. G. G. T. Taylor, J. A. Davies, C. J. Owen, F. Pitout, A. N. Fazakerley, Z. Pu, L. H., Y. V. Bogdanova, Q.-G. Zong, C. Shen, K. Nykyri, B. Lavraud, S. E. Milan, T. D. Phan, H. Rème, E. C. P., C. M. Carr, P. Cargill, M. Lockwood, and B. Sonnerup (2005), Coordinated Cluster/Double Star observations of dayside reconnection signatures, *Ann. Geophys.*, *23*(8), 2867–2875.

Elphic, R. C., M. Lockwood, S. W. H. Cowley, and P. E. Sandholt (1990), Flux transfer events at the magnetopause and in the ionosphere, *Geophys. Res. Lett.*, *17*, 2241–2244, doi:10.1029/GL017i012p02241.

Escoubet, C. P., M. Fehringer, and M. Goldstein (2001), The Cluster mission, *Ann. Geophys.*, *19*, 1197 – 1200.

Farrugia, C. J., R. C. Elphic, D. J. Southwood, and S. W. H. Cowley (1987), Field and flow perturbations outside the reconnected field line region in flux transfer events: Theory, *Planet. Space Sci.*, *35*, 227–240.

Fazakerley, A. N., P. J. Carter, G. Watson, A. Spencer, Y. Q. Sun, J. Coker, P. Coker, D. O. Kataria, D. Fontaine, Z. X. Liu, L. Gilbert, L. He, A. D. Lahiff, B. Mihalčič, S. Szita, M. G. G. T. Taylor, R. J. Wilson, M. Dedieu, and S. J. Schwartz (2005), The Double Star Plasma Electron and Current Experiment, *Ann. Geophys.*, *23*, 2733–2756.

Fear, R. C., A. N. Fazakerley, C. J. Owen, and E. A. Lucek (2005), A survey of flux transfer events observed by Cluster during strongly northward IMF, *Geophys. Res. Lett.*, *32*, L18105, doi:10.1029/2005GL023811.

Fear, R. C., S. E. Milan, A. N. Fazakerley, C. J. Owen, T. Asikainen, M. G. G. T. Taylor, E. A. Lucek, H. Rème, I. Dandouras, and P. W. Daly (2007), Motion of flux transfer events: a test of the Cooling model, *Ann. Geophys.*, *25*, 1669–1690.

Fear, R. C., S. E. Milan, A. N. Fazakerley, E. A. Lucek, S. W. H. Cowley, and I. Dandouras (2008), The azimuthal extent of three flux transfer events, *Ann. Geophys.*, *26*, 2353–2369.

Fear, R. C., S. E. Milan, E. A. Lucek, S. W. H. Cowley, and A. N. Fazakerley (2009), Mixed azimuthal scales of flux transfer events, in *The Cluster Active Archive - Studying the Earth's Space Plasma Environment*, edited by H. Laakso, M. Taylor, and C. P. Escoubet, Astrophysics and Space Science Proceedings, Springer, Dordrecht, doi:???, in press.

Greenwald, R. A., K. B. Baker, J. R. Dudeney, M. Pinnock, T. B. Jones, E. C. Thomas, J.-P. Villain, J.-C. Cerisier, C. Senior, C. Hanuise, R. D. Hunsucker, G. Sofko, J. Koehler, E. Nielsen, R. Pellinen, A. D. M. Walker, N. Sato, and H. Yamagishi (1995), Darn/SuperDARN: A Global View of the Dynamics of High-Lattitude Convection, *Space Sci. Rev.*, *71*, 761–796, doi:10.1007/BF00751350.

Harvey, C. C. (1998), Spatial gradients and the volumetric tensor, in *Analysis Methods for Multi-Spacecraft Data*, edited by G. Paschmann and P. W. Daly, pp. 307–348, ISSI.

de Hoffmann, F., and E. Teller (1950), Magneto-hydrodynamic shocks, *Phys. Rev.*, *80*, 692–703.

Johnstone, A. D., C. Alsop, S. Burdge, P. J. Carter, A. J. Coates, A. J. Coker, A. N. Fazakerley, M. Grande, R. A. Gowen, C. Gurgiolo, B. K. Hancock, B. Narheim, A. Preece, P. H. Sheather, J. D. Winningham, and R. D. Woodliffe (1997), PEACE: A Plasma Electron And Current Experiment, *Space Sci. Rev.*, *79*, 351–398, doi:10.1023/A:1004938001388.

Kawano, H., and C. T. Russell (1996), Survey of flux transfer events observed with the ISEE 1 spacecraft: Rotational polarity and the source region, *J. Geophys. Res.*, *101*(A12), 27,299–27,308.

Kawano, H., and C. T. Russell (1997a), Survey of flux transfer events observed with the ISEE 1 spacecraft: Dependence on the interplanetary magnetic field, *J. Geophys. Res.*, *102*(A6), 11,307–11,314, doi:10.1029/97JA00481.

Kawano, H., and C. T. Russell (1997b), Cause of postterminator flux transfer events, *J. Geophys. Res.*, *102*(A12), 27,029–27,038, doi:10.1029/97JA02139.

Khrabrov, A. V., and B. U. O. Sonnerup (1998), Dehoffmann-teller analysis, in *Analysis Methods for Multi-Spacecraft Data*, edited by G. Paschmann and P. W. Daly, pp. 221–248, ISSI.

King, J. H., and N. E. Papitashvili (2005), Solar wind spatial scales in and comparisons of hourly Wind and ACE plasma and magnetic field data, *J. Geophys. Res.*, *110*(A9), A02104, doi:10.1029/2004JA010649.

Kobel, E., and E. O. Flückiger (1994), A model of the steady state magnetic field in the magnetosheath, *J. Geophys. Res.*, *99*(A12), 23,617–23,622.

Lepping, R. P., M. H. Acũna, L. F. Burlaga, W. M. Farrell, J. A. Slavin, K. H. Schatten, F. Mariani, N. F. Ness, F. M. Neubauer, Y. C. Whang, J. B. Byrnes, R. S. Kennon, P. V. Panetta, J. Scheifele, and E. M. Worley (1995), The Wind Magnetic Field Investigation, *Spa. Sci. Rev.*, *71*, 207–229, doi:10.1007/BF00751330.

Liu, J., V. Angelopoulos, D. Sibeck, T. Phan, Z. Y. Pu, J. McFadden, K. H. Glassmeier, and H. U. Auster (2008), THEMIS observations of the dayside traveling compression region and flows surrounding flux transfer events, *Geophys. Res. Lett.*, *35*, L17S07, doi:10.1029/2008GL033673.

Liu, Z. X., C. P. Escoubet, Z. Pu, H. Laakso, J. K. Shi, C. Shen, and M. Hapgood (2005), The Double Star mission, *Ann. Geophys.*, *23*, 2707–2712.

Lui, A. T. Y., D. G. Sibeck, T. Phan, J. P. McFadden, V. Angelopoulos, and K.-H. Glassmeier (2008), Reconstruction of a flux transfer event based on observations from five THEMIS satellites, *J. Geophys. Res.*, *113*(A12), A00C01, doi:10.1029/2008JA013189.

McFadden, J. P., C. W. Carlson, D. Larson, M. Ludlam, R. Abiad, B. Elliott, P. Turin, M. Marckwordt, and V. Angelopoulos (2008), The THEMIS ESA plasma instrument and in-flight calibration, *Space Sci. Rev.*, *141*, 277–302, doi:10.1007/s11214-008-9440-2.

McWilliams, K. A., T. K. Yeoman, and G. Provan (2000), A statistical survey of dayside pulsed ionospheric flows as seen by the CUTLASS Finland HF radar, *Ann. Geophys.*, *18*, 445–453, doi:10.1007/s005850050902.

McWilliams, K. A., G. J. Sofko, T. K. Yeoman, S. E. Milan, D. G. Sibeck, T. Nagai, T. Mukai, I. J. Coleman, T. Hori, and F. J. Rich (2004), Simultaneous observations of magnetopause flux transfer events and of their associated signatures at ionospheric altitudes, *Ann. Geophys.*, *22*, 2181–2199.

Milan, S. E., T. K. Yeoman, M. Lester, E. C. Thomas, and T. B. Jones (1997), Initial backscatter occurrence statistics from the CUTLASS HF radars, *Ann. Geophys.*, *15*, 703–718, doi:10.1007/s005850050486.

Milan, S. E., M. Lester, S. W. H. Cowley, J. Moen, P. E. Sandholt, and C. J. Owen (1999a), Meridian-scanning photometer, coherent HF radar, and magnetometer observations of the cusp: a case study, *Ann. Geophys.*, *17*, 159–172, doi:10.1007/s005850050746.

Milan, S. E., M. Lester, R. A. Greenwald, and G. Sofko (1999b), The ionospheric signature of transient dayside reconnection and the associated pulsed convection return flow, *Ann. Geophys.*, *17*, 1166–1171.

Milan, S. E., M. Lester, S. W. H. Cowley, and M. Brittnacher (2000), Convection and auroral response to a southward turning of the IMF: Polar UVI, CUTLASS, and IMAGE signatures of transient magnetic flux transfer at the magnetopause, *J. Geophys. Res.*, *105*, 15,741–15,756, doi:10.1029/2000JA900022.

Moen, J., P. E. Sandholt, M. Lockwood, W. F. Denig, U. P. Løvhaug, B. Lybekk, A. Egeland, D. Opsvik, and E. Friis-Christensen (1995), Events of enhanced convection and related auroral activity, *J. Geophys. Res.*, *100*, 23,917–23,934.

Neudegg, D. A., S. W. H. Cowley, K. A. McWilliams, M. Lester, T. K. Yeoman, J. Sigwarth, G. Haerendel, W. Baumjohann, U. Auster, K.-H. Fornacon, and E. Georgescu (2001), The UV aurora and ionospheric flows during flux transfer events, *Ann. Geophys.*, *19*, 179–188.

Owen, C. J., A. N. Fazakerley, P. J. Carter, A. J. Coates, I. C. Krauklis, S. Szita, M. G. G. T. Taylor, P. Travnicek, G. Watson, R. J. Wilson, A. Balogh, and M. W. Dunlop (2001), Cluster PEACE observations of electrons during magnetospheric flux transfer events, *Ann. Geophys.*, *19*, 1509–1522.

Paschmann, G., and B. U. O. Sonnerup (2008), Proper frame determination and walén test, in *Multi-Spacecraft Analysis Methods Revisited*, edited by G. Paschmann and P. W. Daly, pp. 65–74, ISSI.

Paschmann, G., G. Haerendel, I. Papamastorakis, N. Sckopke, S. J. Bame, J. T. Gosling, and C. T. Russell (1982), Plasma and magnetic field characteristics of magnetic flux transfer events, *J. Geophys. Res.*, *87*, 2159–2168.

Paschmann, G., W. Baumjohann, N. Sckopke, I. Papamastorakis, and C. W. Carlson (1986), The magnetopause for large magnetic shear - AMPTE/IRM observations, *J. Geophys. Res.*, *91*, 11,099–11,115, doi:10.1029/JA091iA10p11099.

Phan, T., M. Dunlop, G. Paschmann, B. Klecker, J. Bosqued, H. Rème, A. Balogh, C. Twitty, F. Mozer, C. Carlson, C. Mouikis, and L. Kistler (2004), Cluster observations of continuous reconnection at the magnetopause under steady interplanetary magnetic field conditions, *Ann. Geophys.*, *22*, 2355–2367.

Pinnock, M., A. S. Rodger, J. R. Dudeney, K. B. Baker, P. T. Newell, R. A. Greenwald, and M. E. Greenspan (1993), Observations of an enhanced convection channel in the cusp ionosphere, *J. Geophys. Res.*, *98*, 3767–3776.

Pinnock, M., A. S. Rodger, J. R. Dudeney, F. Rich, and K. B. Baker (1995), High spatial and temporal resolution observations of the ionospheric cusp, *Ann. Geophys.*, *13*, 919–925.

Provan, G., T. K. Yeoman, and S. E. Milan (1998), CUTLASS Finland radar observations of the ionospheric signatures of flux transfer events and the resulting plasma flows, *Ann. Geophys.*, *16*, 1411–1422.

Rème, H., I. Dandouras, C. Aoustin, J. M. Bosqued, J. A. Sauvaud, C. Vallat, P. Escoubet, J. B. Cao, J. Shi, M. B. Bavassano-Cattaneo, G. K. Parks, C. W. Carlson, Z. Pu, B. Klecker, E. Moebius, L. Kistler, A. Korth, R. Lundin, and the HIA Team (2005), The HIA instrument on board the Tan Ce 1 Double Star near-equatorial spacecraft and its first results, *Ann. Geophys.*, *23*, 2757–2774.

Retinò, A., M. B. Bavassano Cattaneo, M. F. Marcucci, A. Vaivads, M. André, Y. Khotyaintsev, T. Phan, G. Pallocchia, H. Rème, E. Möbius, B. Klecker, C. W. Carlson, M. McCarthy, A. Korth, R. Lundin, and A. Balogh (2005), Cluster multispacecraft observations at the high-latitude duskside magnetopause: implications for continuous and component magnetic reconnection, *Ann. Geophys.*, *23*, 461–473.

Rijnbeek, R. P., S. W. H. Cowley, D. J. Southwood, and C. T. Russell (1984), A survey of dayside flux transfer events observed by ISEE-1 and ISEE-2 magnetometers, *J. Geophys. Res.*, *89*, 786–800.

Roelof, E. C., and D. G. Sibeck (1993), Magnetopause shape as a bivariate function of interplanetary magnetic field B_Z and solar wind dynamic pressure, *J. Geophys. Res.*, *98*(A12), 21,421–21,450.

Ruohoniemi, J. M., and K. B. Baker (1998), Large-scale imaging of high-latitude convection with Super Dual Auroral Radar Network HF radar observations, *J. Geophys. Res.*, *103*, 20,797–20,811, doi:10.1029/98JA01288.

Russell, C. T., and R. C. Elphic (1978), Initial ISEE magnetometer results: Magnetopause observations, *Space Sci. Rev.*, *22*, 681–715, doi:10.1007/BF00212619.

Russell, C. T., and R. C. Elphic (1979), ISEE observations of flux transfer events at the dayside magnetopause, *Geophys. Res. Lett.*, *6*, 33–36.

Russell, C. T., M. M. Mellott, E. J. Smith, and J. H. King (1983), Multiple spacecraft observations of interplanetary shocks: Four spacecraft determination of shock normals, *J. Geophys. Res.*, *88*, 4739–4748.

Russell, C. T., J. Berchem, and J. G. Luhmann (1985), On the source region of flux transfer events, *Adv. Space Res.*, *5*, 363–368.

Sandholt, P. E., C. S. Deehr, A. Egeland, B. Lybekk, R. Viereck, and G. J. Romick (1986), Signatures in the dayside aurora of plasma transfer from the magnetosheath, *J. Geophys. Res.*, *91*, 10,063–10,079.

Sandholt, P. E., M. Lockwood, W. F. Denig, R. C. Elphic, and S. Leontjev (1992), Dynamical auroral structure in the vicinity of the polar cusp: Multipoint observations during southward and northward IMF, *Ann. Geophys.*, *10*, 483–497.

Saunders, M. A., C. T. Russell, and N. Sckopke (1984), Flux transfer events: Scale size and interior structure, *Geophys. Res. Lett.*, *11*, 131–134.

Sibeck, D. G., M. Kuznetsova, V. Angelopoulos, K.-H. Glaßmeier, and J. P. McFadden (2008), Crater FTEs: Simulation results and THEMIS observations, *Geophys. Res. Lett.*, *35*, L17S06, doi:10.1029/2008GL033568.

Sonnerup, B. U. O., and L. J. Cahill, Jr. (1967), Magnetopause structure and attitude from Explorer 12 observations, *J. Geophys. Res.*, *72*, 171–183.

Sonnerup, B. U. O., and M. Scheible (1998), Minimum and maximum variance analysis, in *Analysis Methods for Multi-Spacecraft Data*, edited by G. Paschmann and P. W. Daly, pp. 185–220, ISSI.

Sonnerup, B. U. O., I. Papamastorakis, G. Paschmann, and H. Lühr (1987), Magnetopause properties from AMPTE/IRM observations of the convection electric field: Method development, *J. Geophys. Res.*, *92*, 12,137–12,159, doi:10.1029/JA092iA11p12137.

Southwood, D. J., M. A. Saunders, M. W. Dunlop, W. A. C. Mier-Jedrzejowicz, and R. P. Rijnbeek (1986), A survey of flux transfer events recorded by the UKS spacecraft magnetometer, *Planet. Space Sci.*, *34*(12), 1349–1359.

Spreiter, J. R., A. L. Summers, and A. Y. Alksne (1966), Hydromagnetic flow around the magnetosphere, *Planet. Spa. Sci.*, *14*, 223–253.

Walén, C. (1944), On the Theory of Sunspots, *Ark. Mat. Astron. Fys.*, *30*, 1–87.

Wang, Y. L., R. C. Elphic, B. Lavraud, M. G. G. T. Taylor, J. Birn, J. Raeder, C. T. Russell, H. Kawano, Q.-G. Zong, H. Zhang, X. X. Zhang, and R. H. Friedel (2005), Initial results of high-latitude magnetopause and low-latitude flank flux transfer events from 3 years of Cluster observations, *J. Geophys. Res.*, *110*(A9), A11221, doi:10.1029/2005JA011150.

Wild, J. A., S. W. H. Cowley, J. A. Davies, H. Khan, M. Lester, S. E. Milan, G. Provan, T. K. Yeoman, A. Balogh, M. W. Dunlop, K.-H. Fornaçon, and E. Georgescu (2001), First simultaneous observations of flux transfer events at the high-latitude magnetopause by the Cluster spacecraft and pulsed radar signatures in the conjugate ionosphere by the CUTLASS and EISCAT radars, *Ann. Geophys.*, *19*, 1491–1508.

Wild, J. A., S. E. Milan, S. W. H. Cowley, J. M. Bosqued, H. Rème, T. Nagai, S. Kokubun, Y. Saito, T. Mukai, J. A. Davies, B. M. A. Cooling, A. Balogh, and P. W. Daly (2005), Simultaneous in-situ observations of the signatures of dayside reconnection at the high- and low-latitude magnetopause, *Ann. Geophys.*, *23*, 445–460.

Wild, J. A., S. E. Milan, J. A. Davies, M. W. Dunlop, D. M. Wright, C. M. Carr, A. Balogh, H. Rème, A. N. Fazakerley, and A. Marchaudon (2007), On the location of dayside magnetic reconnection during an interval of duskward oriented IMF, *Ann. Geophys.*, *25*, 219–238.

Xiao, C. J., Z. Y. Pu, Z. W. Ma, S. Y. Fu, Z. Y. Huang, and Q. G. Zong (2004), Inferring of flux rope orientation with the minimum variance analysis technique, *J. Geophys. Res.*, *109*, A11218, doi:10.1029/2004JA010594.

Zhang, H., K. K. Khurana, M. G. Kivelson, V. Angelopoulos, Z. Y. Pu, Q.-G. Zong, J. Liu, and X.-Z. Zhou (2008), Modeling a force-free flux transfer event probed by multiple Time History of Events and Macroscale Interactions during Substorms (THEMIS) spacecraft, *J. Geophys. Res.*, *113*(A12), A00C05, doi:10.1029/2008JA013451.

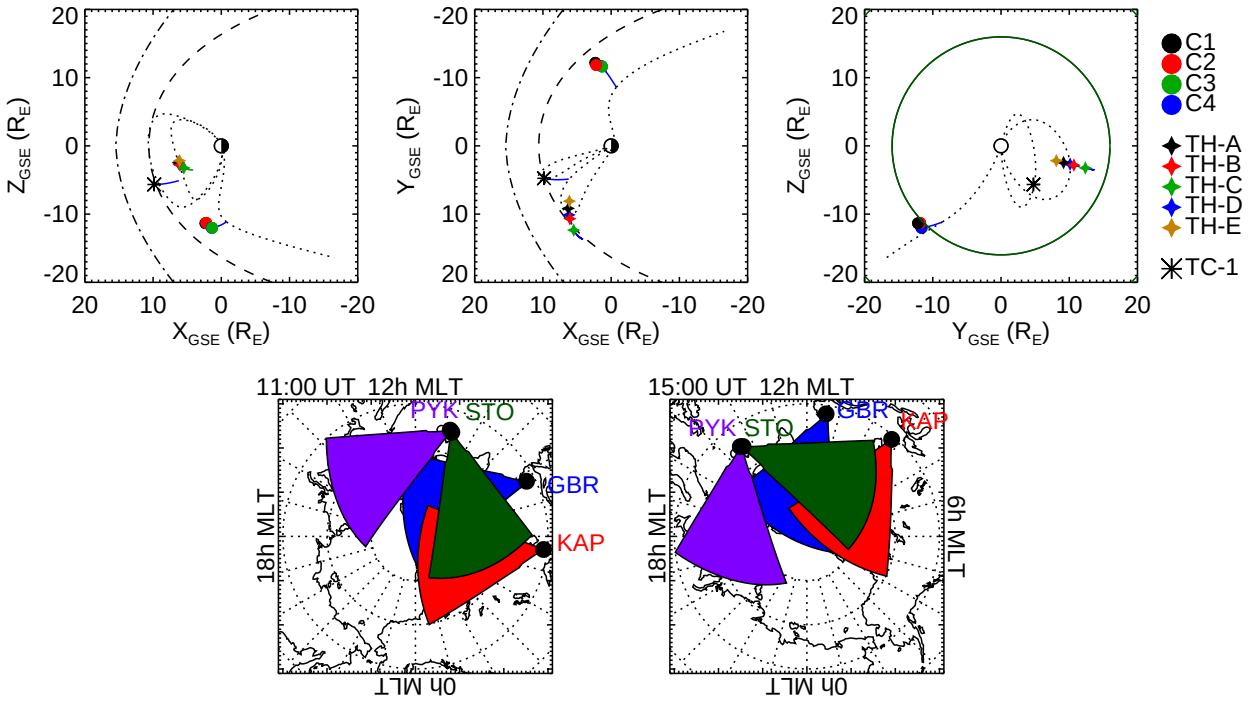

Figure 1: Top: The location of the THEMIS, Cluster and Double Star TC-1 spacecraft. The symbols indicate the locations of the spacecraft at 11:00 UT, and the solid lines show the spacecraft trajectories between 11:00 and 15:00 UT. The dashed and dot-dashed lines represent cuts of the model magnetopause and bow shock respectively. The dotted lines are model field lines that intersect the locations of the spacecraft at 11:00 UT (THEMIS), 12:00 UT (TC-1) and 15:00 UT (Cluster). Bottom: the fields of view of the Þykvibær (PYK), Stokkseyri (STO), Goose Bay (GBR) and Kapuskasing (KAP) radars, at 11:00 and 15:00 UT. The concentric dotted circles represent magnetic latitude (at 10° intervals), and the radial dotted lines represent integer hours of magnetic local time.

Table 1: Results of minimum variance analysis on the flux transfer events observed by all five THEMIS spacecraft. The minimum variance eigenvector is an estimator of the flux tube orientation, and is quoted in boundary normal coordinates. Results from weak B_N signatures are marked by italics.

Time	Spacecraft	Min. Var. Eigenvector	$\lambda_{int}/\lambda_{min}$
14:34 UT	TH-A	(0.926,-0.011,-0.378)	2.15
	TH-B	(0.893,0.167,-0.419)	1.66
	TH-C	(0.315,0.724,-0.614)	2.09
	TH-D	(0.929,0.043,-0.368)	1.99
	TH-E	(0.921,-0.049,-0.386)	2.20
14:42 UT	TH-A	(0.962,-0.272,-0.019)	2.54
	TH-B	*(0.644,0.620,0.499)*	*2.11*
	TH-C	*(0.495,0.743,-0.450)*	*1.70*
	TH-D	*(0.417,0.900,-0.125)*	*1.49*
	TH-E	(0.638,0.725,-0.260)	1.34

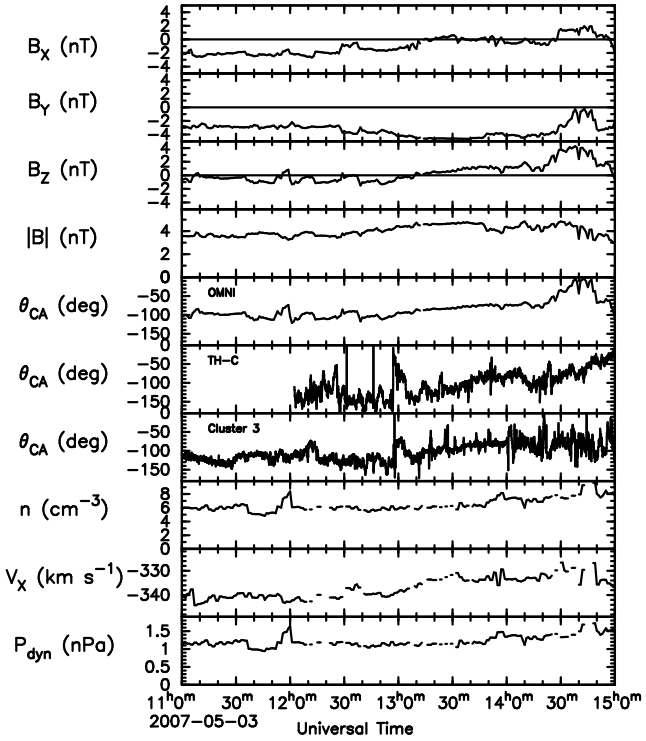

Figure 2: Solar wind conditions observed by the Wind satellite (OMNI high resolution data set) and the clock angle observed by Cluster 3 and THEMIS-C (after 12:02 UT), which were situated in the magnetosheath.

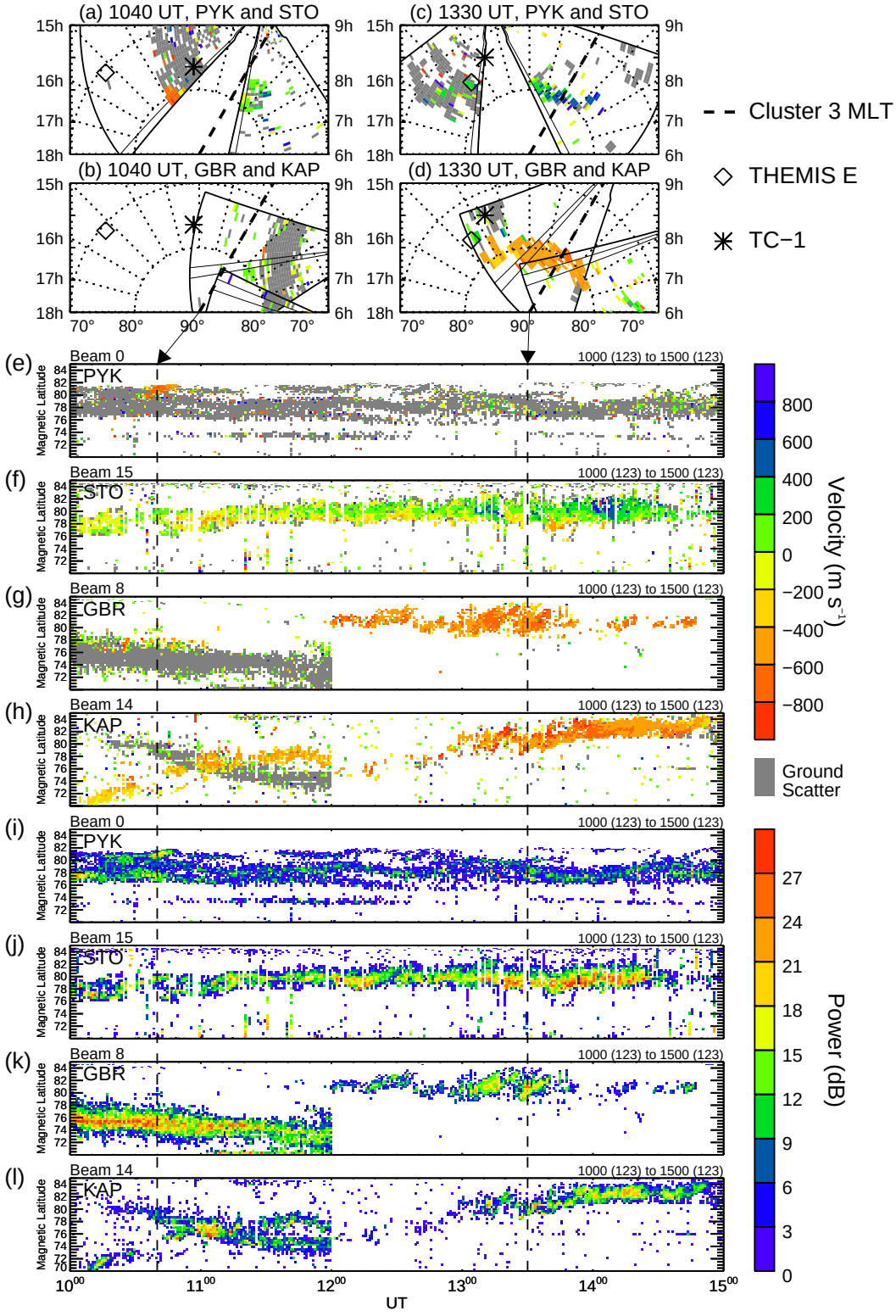

Figure 3: Observations from four SuperDARN radars. (a-d) Spatial views of the ionospheric velocity deduced from dayside radar backscatter at 10:40 UT (a & b) and 13:30 UT (c & d) by the Þykvibær and Stokkseyri radars (a & c) and by the Goose Bay and Kapuskasing radars (b & d). The grid shown represents magnetic latitude (70° to 90° - dotted circular lines) and magnetic local time (6h to 18h - dotted radial lines). The symbols indicate the footprints of the THEMIS and TC-1 spacecraft (in panels (a) and (b) the TC-1 footprint was calculated using the position of the spacecraft after its 11:30 UT magnetopause crossing), and a thick dashed line indicates the magnetic local time of the footprint of Cluster 3 after its magnetopause crossing at 16:10 UT. (e-h) Time series of the ionospheric velocity for one beam for each radar as a function of magnetic latitude: (e) Þykvibær, (f) Stokkseyri, (g) Goose Bay and (h) Kapuskasing. (i-l) Corresponding time series of radar backscatter power.

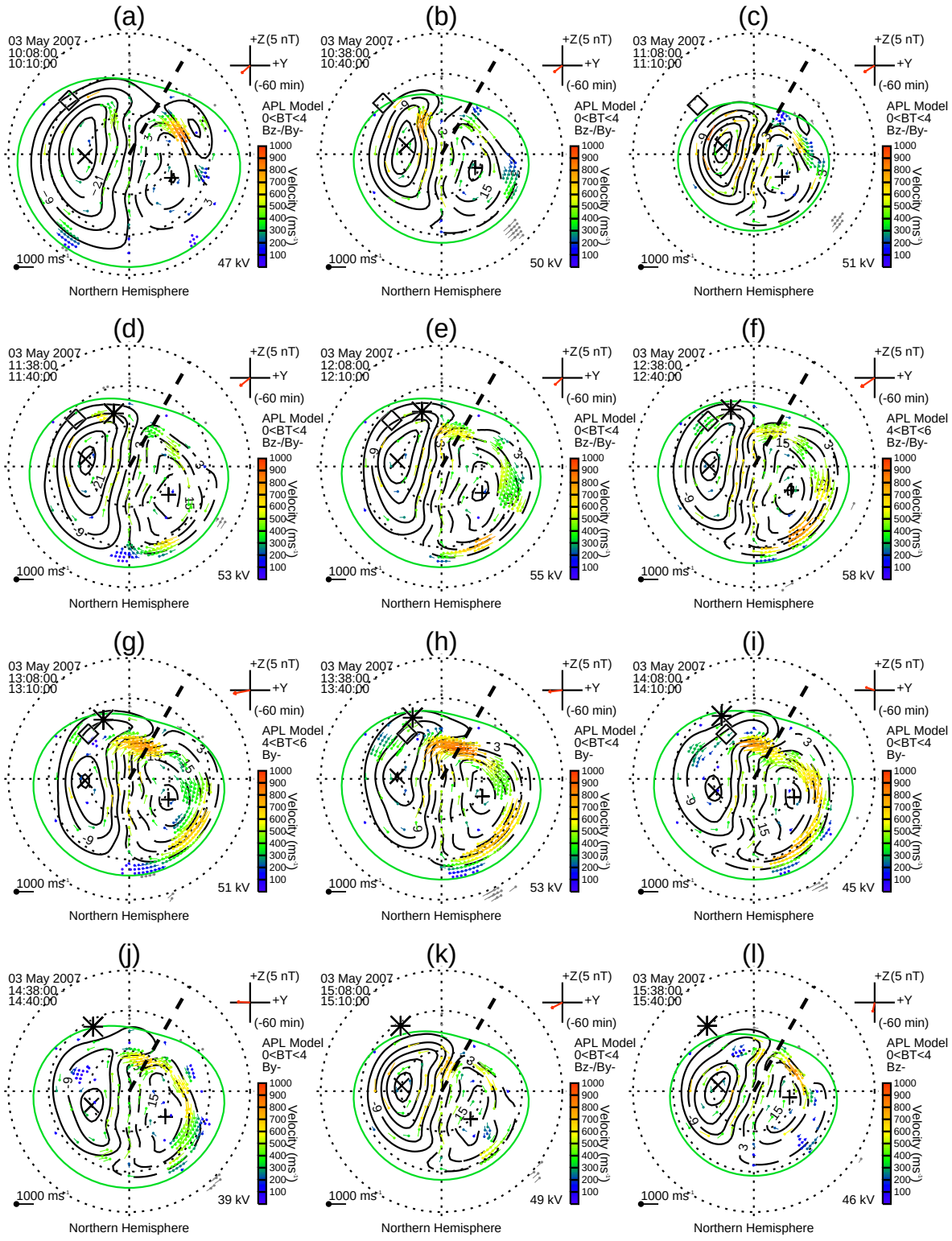

Figure 4: Two-dimensional model fit of the observed ionospheric flows. Each panel shows the ionospheric flows observed by each of the Northern Hemisphere SuperDARN radars, fitted to the map potential model. The black contours are the ionospheric electric potential, based on a statistical model but fitted to the observed flows (where observations are available). Coloured points indicate 'true' velocity vectors, which are the combination of the observed ionospheric velocities (line-of-sight components) with and the component perpendicular to the line of sight derived from the ionospheric potential model. The diamond and asterisk represent the footprints of THEMIS-E and TC-1, and the dashed radial line represents the magnetic local time of the footprint of Cluster 3 after its 16:10 UT magnetopause crossing.

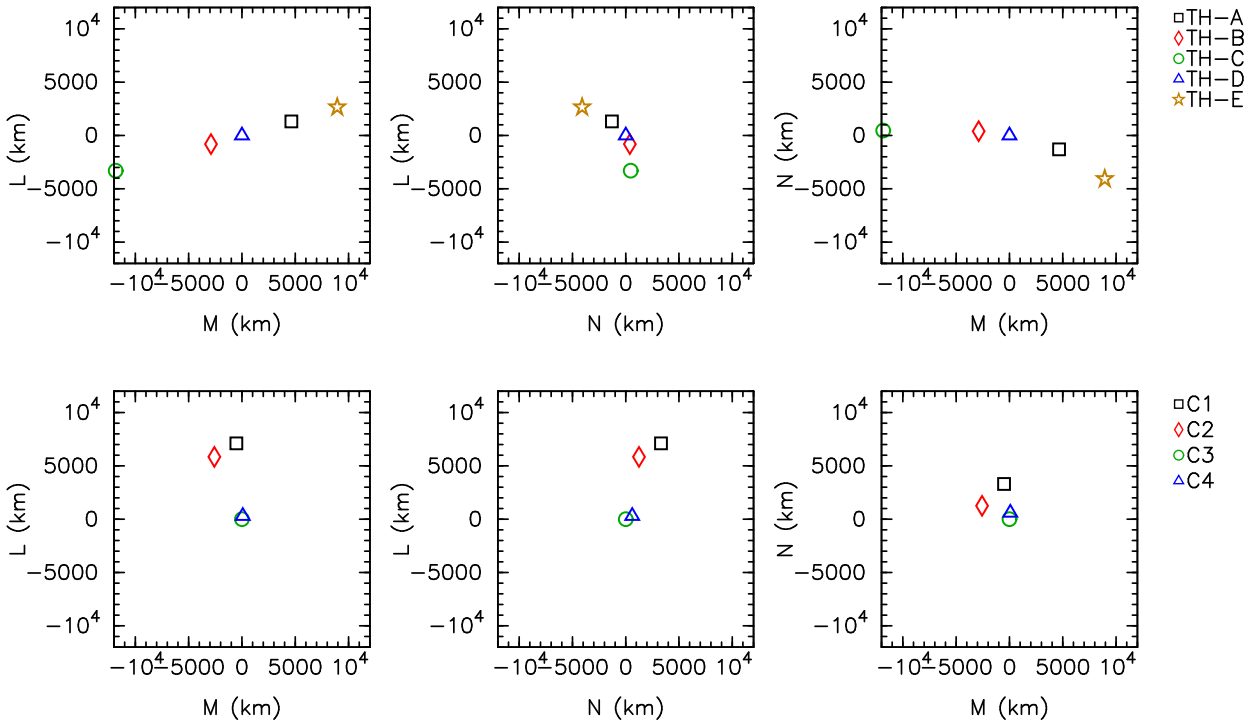

Figure 5: The orientation of the THEMIS (top row) and Cluster (bottom row) spacecraft at 13:00 UT in boundary normal coordinates. The THEMIS spacecraft were aligned in a string which straddled the magnetopause and also extended along the magnetopause; the Cluster spacecraft were oriented in an elongated triangle, with Clusters 3 and 4 close together, both separated by less than 7800 km from Clusters 1 and 2.

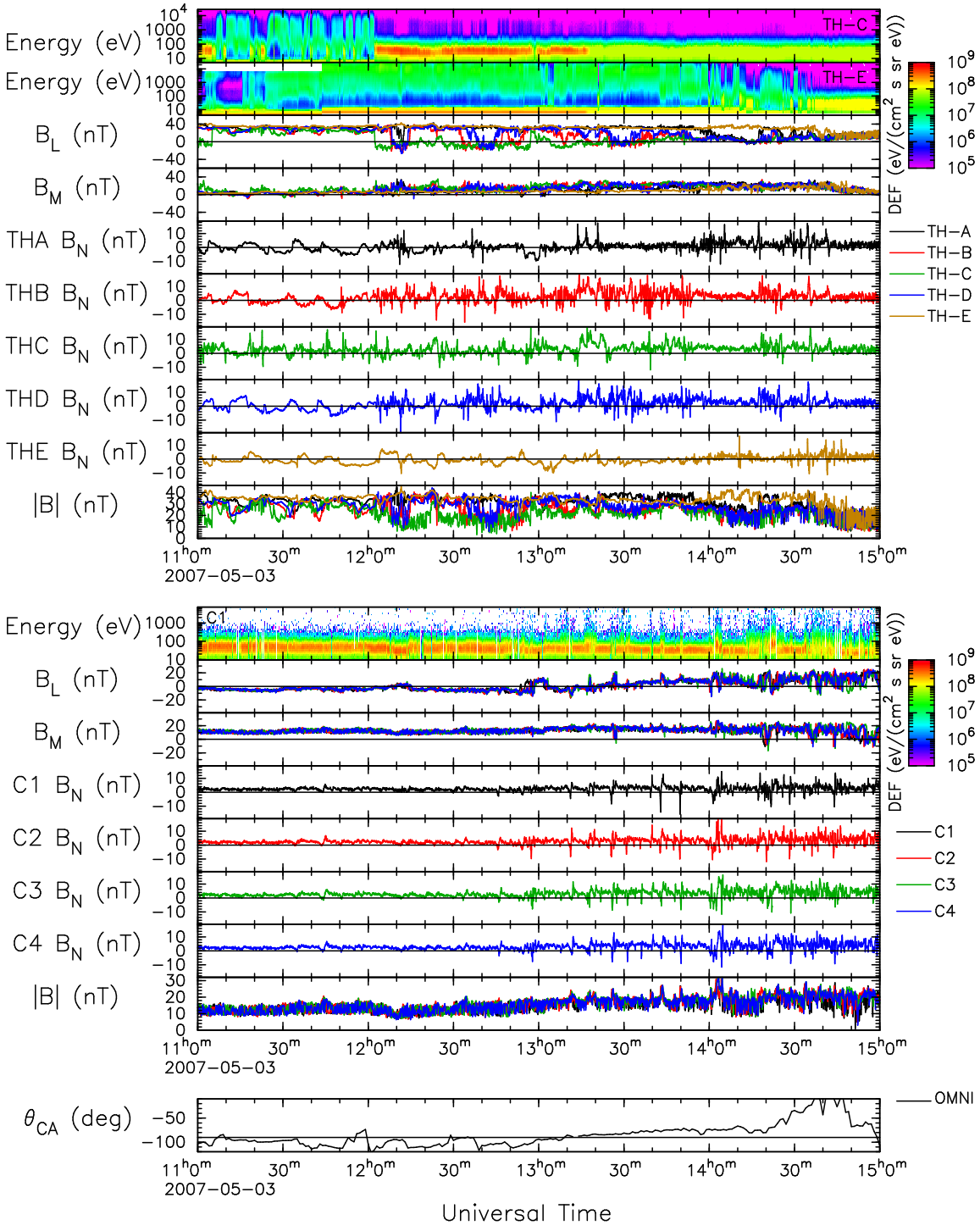

Figure 6: Electron and magnetic field observations by the THEMIS quintet (top) and Cluster quartet (middle) of spacecraft. The top two panels show electron spectrograms (omnidirectional spectra from TH-C & TH-E, and parallel pitch-angles from Cluster 1), the magnetic field observed by all spacecraft tangential to the magnetopause (B_L and B_M), the normal components of the magnetic field for each spacecraft (B_N) and the magnetic field strength $|B|$. The bottom panel shows the IMF clock angle from Figure 2.

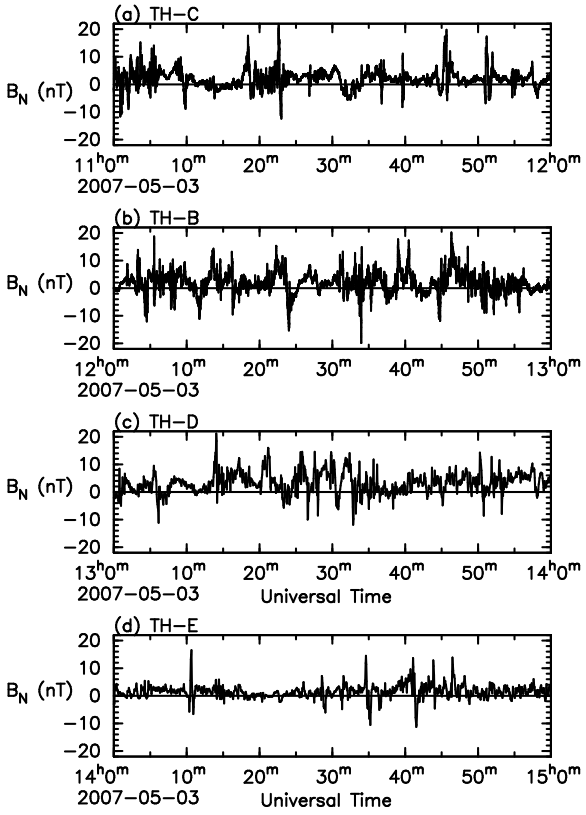

Figure 7: Enlargements of the B_N traces in Figure 6. (a) TH-C, 11:00 to 12:00 UT (4 Hz data). (b) TH-B, 12:00 to 13:00 UT (4 Hz). (c) TH-D, 13:00 to 14:00 UT (3 s) (d) TH-E, 14:00 to 15:00 UT (3 s).

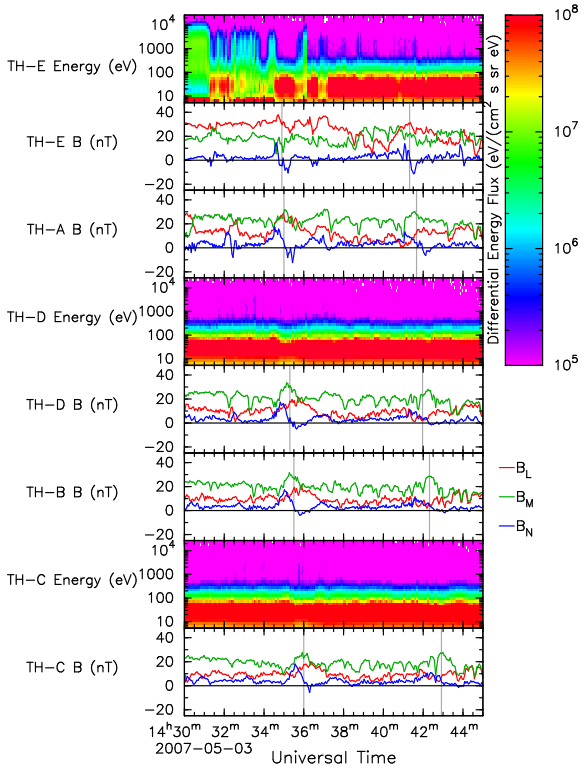

Figure 8: Two FTEs which were observed by all THEMIS spacecraft. The spacecraft are ordered by position of the spacecraft along the magnetopause. Spectrograms are omnidirectional spectra of the electron differential energy flux observed by TH-C, D and E, and line traces are the B_L, B_M and B_N components observed by all five spacecraft.

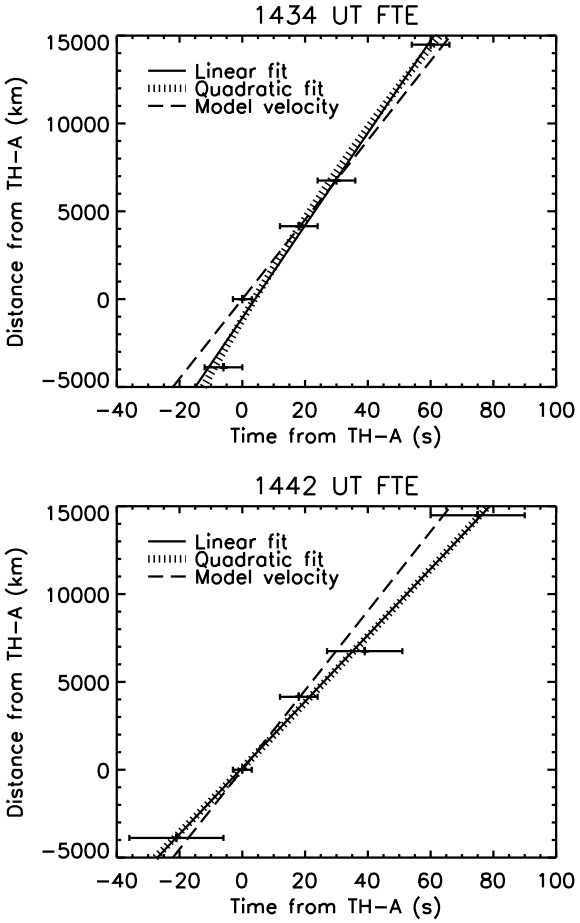

Figure 9: Multi spacecraft timing analysis. Each plot shows the time between the FTE being observed at TH-A and each of the other spacecraft against the separation of the spacecraft in the magnetopause plane. The solid line in each panel is a linear best fit; the hatched line is a quadratic best fit and the dashed line is a straight line whose gradient is the speed given by the Cooling model discussed in Section 4.

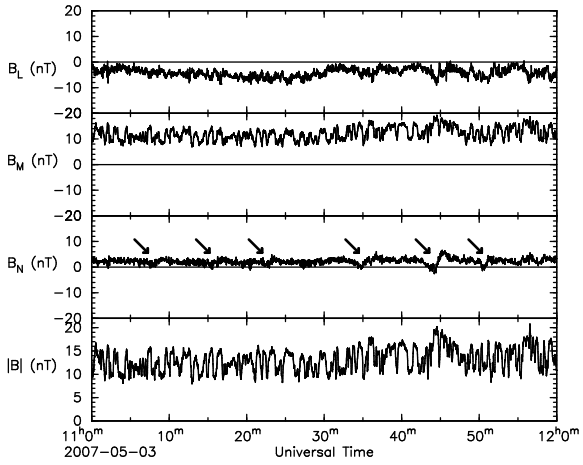

Figure 10: Reverse polarity FTEs observed by Cluster 3 between 11:00 and 12:00 UT.

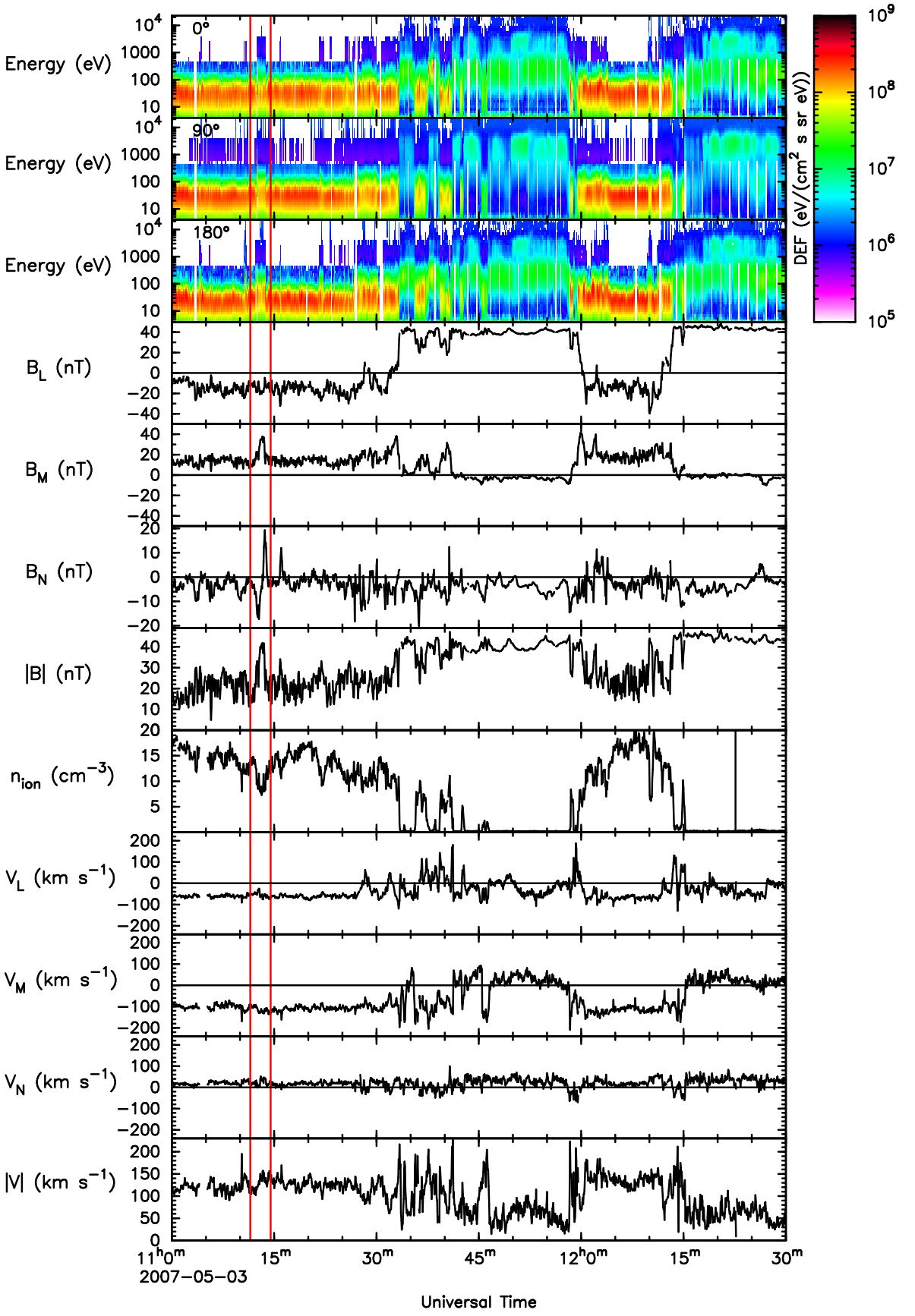

Figure 11: Electron and magnetic field observations from TC-1. From top: electron spectrograms for pitch angles parallel, perpendicular and antiparallel to the magnetic field, the magnetic field and ion moments in boundary normal coordinates. The red lines indicate an FTE observed by TC-1.

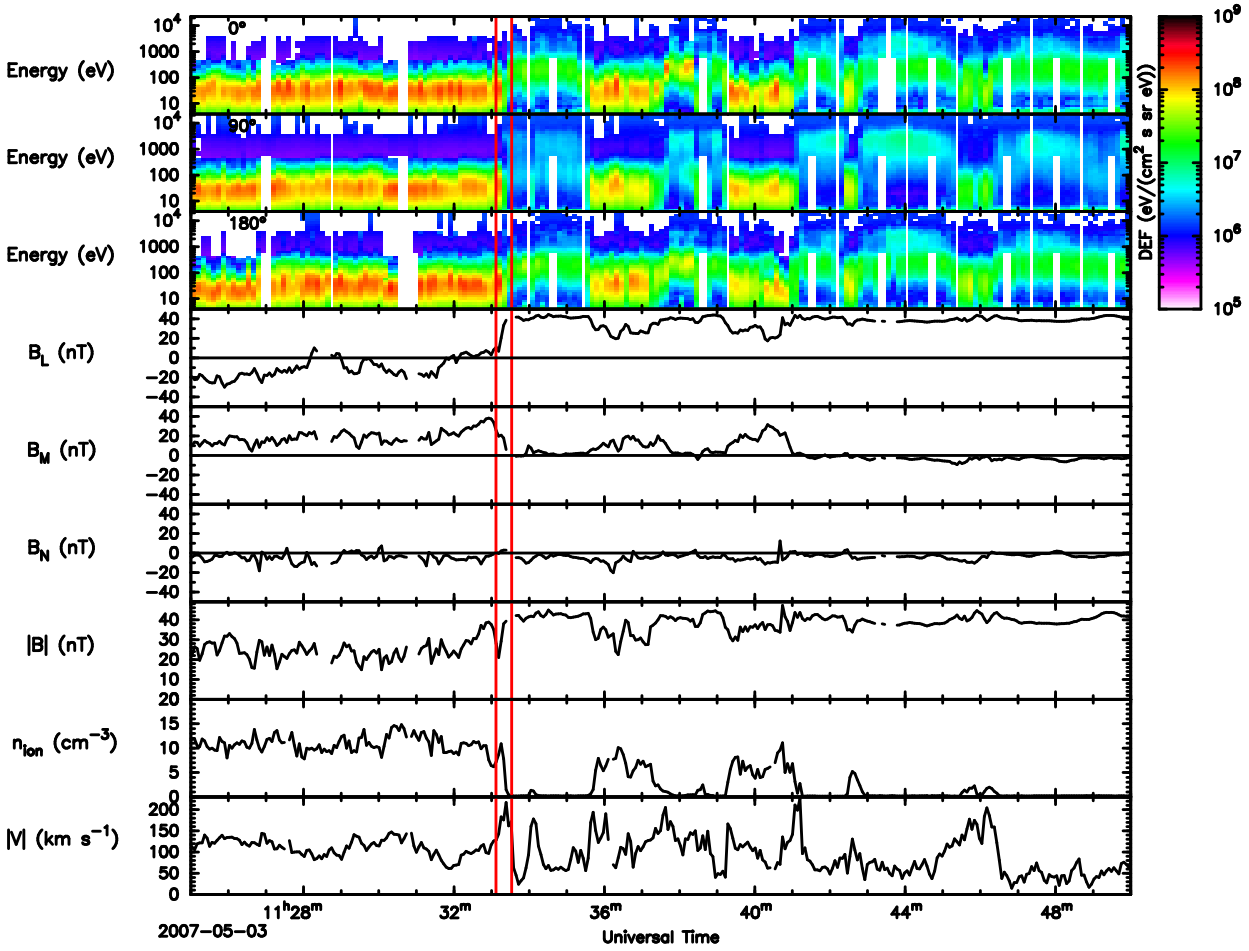

Figure 12: The electron spectra, magnetic field and the ion bulk speed observed by TC-1 at the magnetopause. The red lines indicate the interval used for the Walén test in Figure 13.

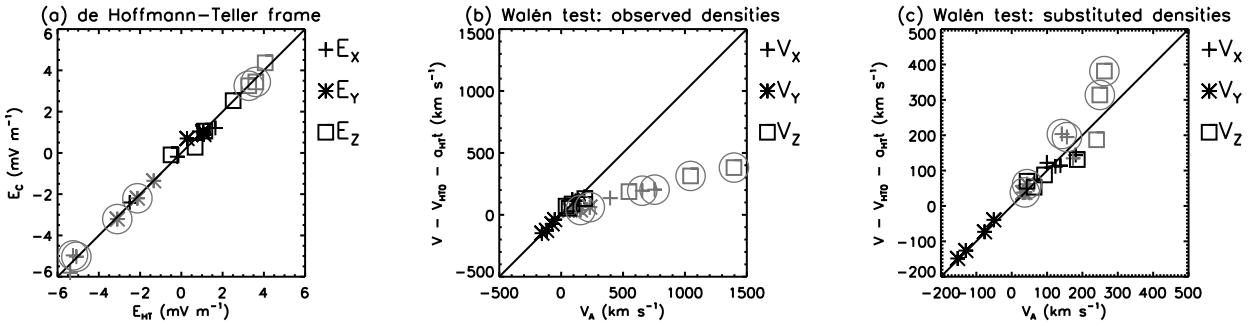

Figure 13: The results of the Walén test carried out on data between 11:33:07 and 11:33:32 UT. (a) The electric field caused by magnetic field convection observed in the GSE frame ($\mathbf{E}_C = -\mathbf{v} \times \mathbf{B}$, where $\mathbf{v}$ is the ion bulk velocity) plotted against the electric field induced by the accelerating de Hoffmann-Teller (dHT) frame ($\mathbf{E}_{HT} = -\mathbf{V}_{HT} \times \mathbf{B}$, where $\mathbf{v}_{HT}$ is the time-varying velocity of the frame in GSE coordinates). The good correlation between the two quantities shows that the selected transformation has correctly identified the dHT frame. (b) The ion bulk velocity in the dHT frame plotted against the Alfvén velocity, which is calculated using the observed ion density. Points corresponding to a density lower than 1.5 cm^{-3} are shaded gray, and points using interpolated magnetic field measurements are encircled. The flows observed in higher-density regions are at the Alfvén velocity in the dHT frame, and can therefore be identified as reconnection jets. The flows observed in this interval whilst the density is low are also faster than the magnetosheath velocity, but the calculated Alfvén velocities are higher than the observed flows. (c) The ion bulk velocity in the dHT frame plotted against the Alfvén velocity calculated using the substitution $\rho = \rho_1(1-\alpha_1)/(1-\alpha)$

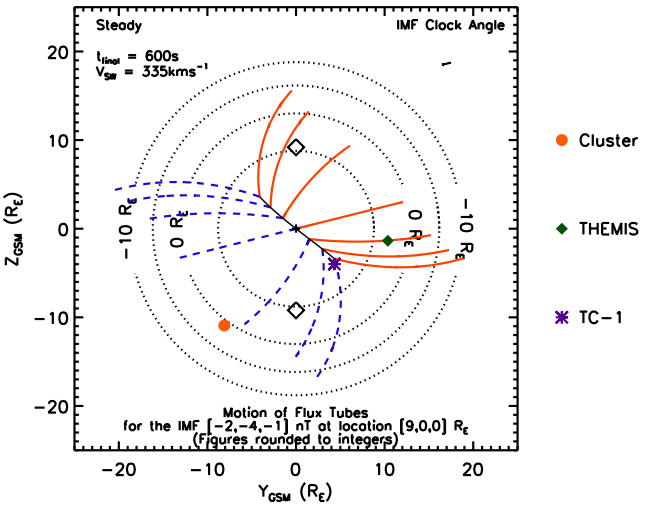

Figure 14: Expected paths of open magnetic field lines determined from the Cooling model, based on IMF parameters at 11:13 UT. Concentric dashed circles are contours in X_{GSM}. The black line in the centre represents an X-line initiated at the subsolar point with arbitrary length of 12 R_E. The solid and dashed lines emanating from the X-line are the model FTE paths for flux tubes connected to the Northern and Southern Hemisphere respectively. The cusps are treated as points (unfilled diamonds) and the locations of the Cluster, THEMIS and TC-1 spacecraft, projected onto the model magnetopause, are indicated.